NTNU
Norwegian University of
Science and Technology

Characterization of a *Paxx* Knockout Mouse Model

Growth and immune system development in
mice deficient of DNA repair factor PAXX

Siri Sæterstad

Biotechnology (5 year)
Submission date: June 2018
Supervisor: Per Bruheim, IBT
Co-supervisor: Valentyn Oksenych, Institutt for kreftforskning og molekylær medisin

Norwegian University of Science and Technology
Department of Biotechnology and Food Science

Acknowledgement

This project was written as an external master thesis in Molecular Medicine, as part of a MSc in Biotechnology at the Department of Biotechnology and Food Science (Faculty of Natural Sciences, NTNU, Trondheim). The master thesis was conducted at the Department of Clinical and Molecular Medicine (Faculty of Medicine and Health Sciences, NTNU, Trondheim) in the Non-Homologous End-Joining group headed by Valentyn Oksenych, PhD.

I want to thank my supervisor, Valentyn Oksenych, for both challenging and encouraging me**,** and for the close follow-up, help, and advice provided throughout my master thesis. I appreciate all the knowledge you've shared, and your willing to help me succeed during the past year. I am grateful that I've been trusted with responsibility, and value the opportunities I've been given.

To all members of our group and others working in the lab - thank you for helping me out whenever needed, and for teaching me your ways. A special thanks to Mengtan Xing and Raquel Gago-Fuentes for always reaching out a helping hand.

Nina-Beate Liabakk, thank you for all help regarding flow cytometry, and for being patient when the protocols didn't work as expected. I appreciate your willing to make it work, which it finally did. A huge thank you to Antonio Sarno for technical assistance and guidance during my final flow cytometric experiments. I also want to thank Anne Marit Sponaas and Rui Yang for lending us antibodies, and the Comparative Medicine Core Facility (Faculty of Medicine and Health Sciences, NTNU, Trondheim) for providing the final mouse for experiments.

I want to thank my internal supervisor at the Department of Biotechnology and Food Science (Faculty of Natural Sciences, NTNU, Trondheim), Per Bruheim, for support and advice during the past year.

Last but not least – I want to thank my friends and family for all support and encouragement, it has meant a lot to me.

Abstract

Non-Homologous End-Joining (NHEJ) is the major DNA double-strand break (DSB) repair pathway in higher eukaryotes, functional throughout the cell cycle. NHEJ involves a variety of proteins; some are essential, whereas others are accessory factors only required for resolving specific types of lesions. Paralog of XRCC4 and XLF (PAXX) is an accessory factor that is able to interact directly with the NHEJ-determining factor Ku, and have shown to be partly redundant with the XRCC4-Like Factor (XLF). In addition, PAXX has been shown to have a significant impact on the repair of radiation- and chemically-induced DSBs in human, murine, and chicken cells, suggesting an important role of PAXX in NHEJ. However, the functional role of PAXX is still not fully understood. Isolated PAXX- and XLF-deficiencies in previously published mouse models reveal no overt phenotype, whereas a combined deficiency results in embryonic lethality due to extensive apoptosis in the central nervous system. These findings indicate important overlapping functions among these two proteins. The first aim of this project was to investigate the impact of PAXX-deficiency on growth and immune system development in our *Paxx* mouse model. This was done by comparing the lymphoid cell counts, spleen weight, thymus weight, and body weight of our $Paxx^{+/-}$ and $Paxx^{-/-}$ mice to WT and NHEJ-defective mice. To determine the effect of *Paxx*-inactivation on lymphocyte development, B and T cell frequencies in spleen and thymus of PAXX-deficient mice were compared to PAXX-proficient mice. Our *Paxx* knockout mouse model was here found to be indistinguishable from WT mice in relation to growth, lymphoid cell counts in thymus and femoral bone marrow, and lymphocyte development. However, a mild reduction in the number of splenocytes was observed in our *Paxx* knockout mice. This is suggested to be a result of impaired proliferation and/or mild defects in general DNA repair, rather than impairment of lymphocyte development. The second aim of this project was to determine whether crossing *Paxx.Xlf* double heterozygous mice into a p53-background could rescue the lethality of $Paxx^{-/-}Xlf^{/-}$ mice. No $Paxx^{-/-}Xlf^{-/-}Trp53^{+/-}$ or $Paxx^{-/-}Xlf^{-/-}$Trp53$^{-/-}$ mice were identified among the 64 analyzed pups during this project. More mice need to be analyzed before any conclusion about viability of these complex mutants can be made. If these mice prove to be viable, this would allow *in vivo* studies of double-deficient PAXX and XLF mice. Further investigation of overlapping and non-overlapping functions between PAXX and XLF would enhance the current understanding of the functional interaction between these two proteins, and thus the NHEJ pathway in general.

Sammendrag

Non-Homologous End-Joining (NHEJ) er det viktigste reparasjonssporet av dobbelttrådet DNA-brudd («DSBs») i høyere eukaryoter, da det er funksjonelt gjennom hele cellesyklusen. NHEJ involverer en rekke proteiner, hvor noen er helt essensielle, mens andre kun kreves til reparasjon av bestemte typer DNA-skader. Paralog of XRCC4 and XLF (PAXX) er en NHEJ-faktor som interagerer direkte med den NHEJ-avgjørende faktoren Ku, og som har vist seg å ha delvis overlappende funksjoner med XRCC4-Like Factor (XLF). Det har blitt demonstrert at PAXX har en betydelig innvirkning på reparasjon av kjemiske- og strålings-induserte «DSBs» i både menneske-, muse-, og kyllingceller. Dette indikerer at PAXX spiller en viktig, men fortsatt ikke fult ut forstått, rolle i NHEJ. Tidligere publiserte *Paxx*- og *Xlf*-musemodeller har vist at isolerte mangler av XLF eller PAXX ikke medfører en merkbar fenotype i mus, mens kombinert mangel av PAXX og XLF resulterer i embryonal dødelighet grunnet omfattende apoptose i sentralnervesystemet. Dette indikerer viktige overlappende funksjoner mellom disse proteinene. Det første målet i dette prosjektet var å undersøke hvordan PAXX-mangel påvirker vekst og immunsystemutvikling i våre *Paxx*-mus. Dette ble gjort ved å sammenligne antall celler i lymfoide organer, miltvekt, tymusvekt, og kroppsvekt av våre $Paxx^{+/-}$- and $Paxx^{-/-}$-mus med villtypemus og NHEJ-defekte mus. For å undersøke hvorvidt *Paxx*-inaktivering påvirker lymfocyttutvikling i mus, ble B- og T-cellefrekvenser i milt og tymus fra mus med inaktiverte *Paxx* alleler sammenlignet med kontroll-mus. Det ble ikke funnet noen signifikante forskjeller i antall tymus- eller beinmargsceller, vekst, eller lymfocyttutvikling mellom våre *Paxx*-mus og villtypemus. Det ble derimot observert en reduksjon i antall miltceller i $Paxx^{-/-}$ mus, sammenlignet med villtypemus. Denne observasjonen foreslås å være et resultat av nedsatt cellulær proliferasjon og/eller en mild defekt i generell DNA-reparasjon, fremfor hemmet lymfocyttutvikling. Det andre målet i dette prosjektet var å undersøke om inaktivering av p53 kunne redde den embryonale dødeligheten av kombinert PAXX- og XLF-mangel i mus. Ingen $Paxx^{-/-}Xlf^{-/-}Trp53^{+/-}$ eller $Paxx^{-/-}Xlf^{-/-}Trp53^{-/-}$ mus ble identifisert blant 64 analyserte mus i løpet av dette prosjektet. Flere mus må analyseres før det kan trekkes en konklusjon angående levedyktigheten til disse komplekse mutantene. Dersom de skulle vise seg å være levedyktig, vil dette tillate *in vivo*-studier av kombinert PAXX- og XLF-mangel. Videre studier av overlappende og ikke-overlappende funksjoner mellom PAXX og XLF vil øke forståelsen av deres funksjonelle rolle i NHEJ, og dermed forståelsen av NHEJ generelt.

Table of Contents

List of Figures

List of Tables

Abbreviations

Ag	Antigen
AgR	Antigen Receptor
ATM	Ataxia Telangiectasia-Mutated
BCR	B Cell receptor
bp	Base pair
BSA	Bovine Serum Albumin
CD	Cluster of Differentiation
Clic3	Chloride intracellular channel 3
CSR	Class Switch Recombination
D	Diversity
DDR	DNA Damage Response
DN	Double Negative
DNA-PKcs	DNA-dependent Protein Kinase catalytic subunit
DP	Double Positive
DSB	Double-Strand Break
FBS	Fetal Bovine Serum
H-chain	Heavy chain
HR	Homologous Recombination
HRP	Horseradish Peroxidase
HSC	Hematopoietic Stem Cell
Ig	Immunoglobulin
IR	Ionizing Radiation
J	Joining
kDa	Kilodalton
Ku	Ku70/Ku80 heterodimer
L-chain	Light chain
Lig4	DNA Ligase IV
NHEJ	Non-Homologous End-Joining
PAXX	Paralogue of XRCC4 and XLF
PBS	Phosphate-Buffered Saline
PCC	Post-Cleavage Complex
PCR	Polymerase Chain Reaction

RAG1/2	Recombination Activating Gene 1 and 2
RBC	Red Blood Cell
RSS	Recombination Signal Sequence
RT	Room temperature
SCID	Severe Combined Immunodeficiency
SHM	Somatic Hypermutation
SP	Single Positive
SSB	Singe-Strand Break
TBE	Tris-Borate-EDTA
T_C	T Cytotoxic Cell
TCR	T Cell Receptor
T_H	T Helper Cell
Trp53	Transformation related protein 53, gene encoding p53
V	Variable
V(D)J	Variable(Diversity)Joining
WT	Wild Type
XLF	XRCC4-Like Factor
XRCC4	X-ray Repair Cross-Complementing protein 4

1 Introduction

1.1 DNA Repair

Our DNA is continuously exposed to damage by both endogenous and exogenous agents, and the sufficient repair of these lesions is essential to maintain genomic stability. Failure in DNA repair has severe consequences, including susceptibility to cancer development due to chromosomal aberrations, neurological abnormalities, immunodeficiency, and premature cellular aging. DNA damage can result in various forms of single-strand breaks (SSBs) or double-strand breaks (DSBs), and cells have thus evolved a number of DNA repair pathways for resolving distinct lesions. The particular pathway chosen depends on several factors, such as the complexity of the damage, the chromatin state, and the cell cycle stage[1].

1.1.1 DNA Double-Strand Breaks

DSBs are considered to be the most deleterious form of DNA damage, and can arise during normal cellular metabolism, transcription and replication, or as a result of exposure to DNA damaging agents such as ionizing radiation (IR). DSBs are also formed as natural intermediates during V(D)J recombination in developing B and T cells of the mammalian immune system (described in Section 1.2.4), and during class switch recombination (CSR) in activated B cells. There are two main DNA DSB repair pathways; Homologous Recombination (HR) and Non-Homologous End-Joining (NHEJ). HR requires a homologous sister chromatid to be used as a template during repair, restricting HR to the S[A] and G_2[B] phase of the cell cycle. NHEJ do not require a template and is thus functional throughout the cell cycle in both dividing and non-dividing cells. This makes NHEJ the major DSB repair pathway in higher eukaryotes, especially in the G_1[C] and G_0[D] phase when a homologous sister chromatid is unavailable for HR to occur[1].

[A] S: Synthesis phase, DNA replication. The S phase occurs between the G_1 and G_2
[B] G_2: Second gap phase, cell growth. Cells in this phase are preparing for mitosis
[C] G_1: First gap phase, cell growth
[D] G_0: Resting state, non-dividing cells

1.1.2 Non-Homologous End-Joining

In NHEJ, DSBs with little (1-4bp) or no sequence homology are brought together for repair[2]. NHEJ involves four core (essential and evolutionary conserved) factors; the Ku70/Ku80 heterodimer (Ku), DNA Ligase IV (Lig4), and X-ray Repair Cross-Complementing protein 4 (XRCC4)[3]; as well as several accessory factors, including DNA-dependent Protein Kinase catalytic subunit (DNA-PKcs), Artemis (an essential nuclease during V(D)J recombination in developing lymphocytes)[4], XRCC4-Like Factor (XLF), and Paralogue of XRCC4 and XLF (PAXX)[1, 2]. These factors contribute at different stages in the three-step NHEJ pathway, involving: DSB-recognition, end-processing, and ligation. NHEJ is initiated by Ku, acting as a DSB-sensor by binding both ends of the break[1]. Ku70 and Ku80 interact tightly and wrap around one another, forming a ring-shaped structure able to thread onto DNA ends in a sequence-dependent manner. Binding of Ku is a crucial step in NHEJ; a series of interactions, such as DNA-PKcs activation, DNA end-processing, and ligation depend on the initial presence of Ku for NHEJ to proceed. In addition of being a determining factor for NHEJ, Ku also protects DNA ends from non-specific end-processing and degradation, and inhibits other DNA repair pathways such as HR[2]. PAXX has been shown to interact directly with DNA-bound Ku, and is thought to promote assembly and/or stability of the NHEJ machinery by stabilizing Ku at DNA ends[5]. Ku recruits DNA-PKcs at both sides of the break, forming a complex that is proposed to stabilize and align the DNA ends by dimerization of DNA-PKcs[2, 6]. Binding of DNA-PKcs activates its kinase domain, enabling autophosphorylation and phosphorylation of downstream factors[7]. Different factors are required for end-ligation depending on the complexity and nature of the ends; some breaks have 'clean' cohesive or blunt ends that can be ligated directly, whereas other breaks are more complex, in need of processing prior to ligation. Breaks resulting in overhanging ends and/or ends with modifications can be processed by a variety of enzymes, including polymerases, kinases, phosphatases, and nucleases. Once ideal termini are obtained through processing, XLF interacts with the XRCC4-Lig4 complex to complete the final step of the pathway – ligation[2]. A simplified overview of NHEJ is presented in Figure 1.1.

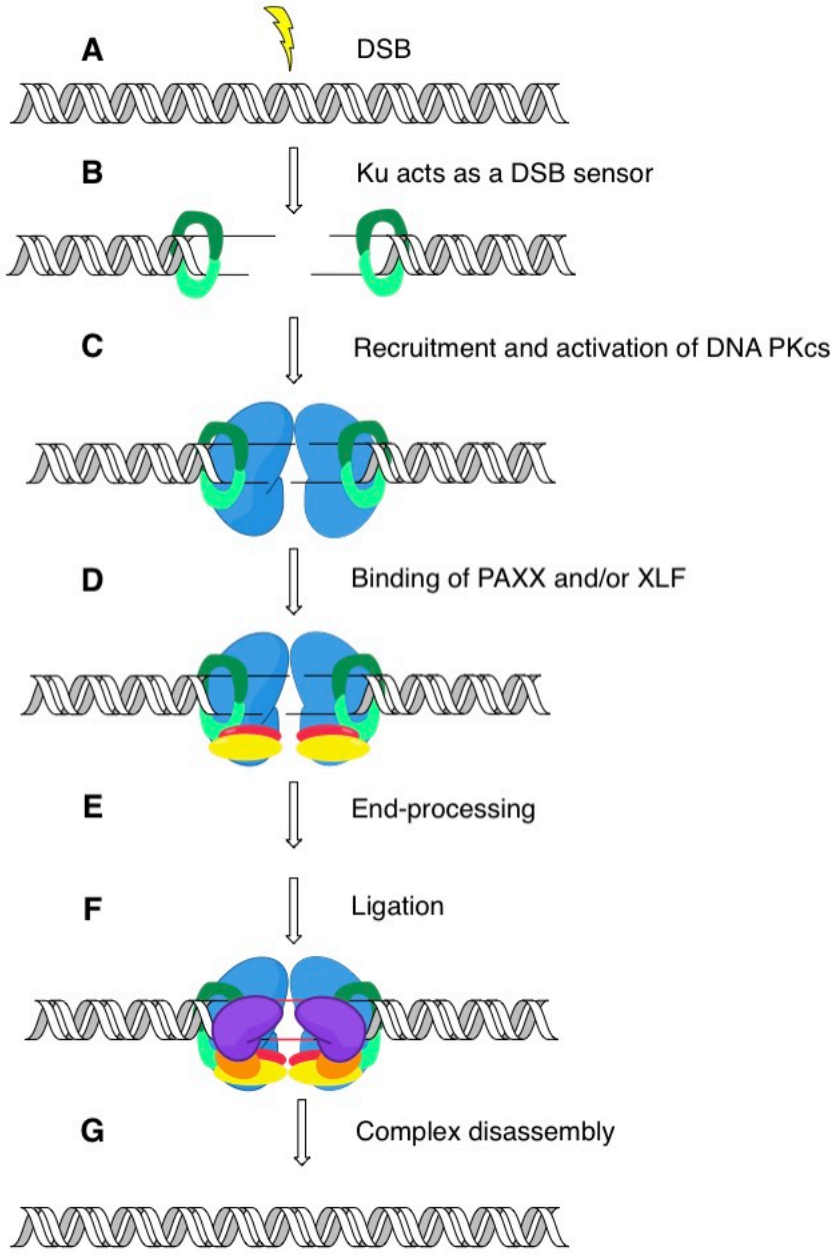

Figure 1.1: Simplified overview of the NHEJ pathway. **A)** DSB generated by endogenous or exogenous agents. **B)** Ku (green) recognize and bind both ends of the break. **C)** DNA-PKcs (blue) is recruited and activated at the site of DSB. **D)** Binding of accessory factors PAXX (red) and/or XLF (yellow). **E)** If the ends are incompatible for direct ligation, end-processing factors are required (*e.g.* the nuclease Artemis). **F)** Once ideal termini are obtained, XLF recruits XRCC4 (orange) in complex with Lig4 (purple) to complete the final step of the pathway – ligation. **G)** Complex disassembly. Figure based on Rulten, S.L. and G.J. Grundy, *Non-homologous end joining: Common interaction sites and exchange of multiple factors in the DNA repair process.* Bioessays, 2017. **39**(3), p. 4.

1.1.3 PAXX and XLF

Two independent research groups reported mammalian XLF (also known as Cernunnos) as a new NHEJ factor in 2006[8, 9]. PAXX (also known as XRCC4-like small protein (XLS) or C9orf142) was reported by three independent research groups in 2015[5, 10, 11]. The PAXX protein is structurally similar to XRCC4 and XLF, all three consisting of a globular head followed by a coiled-coil stalk. Despite structural similarities among these proteins, PAXX share little sequence homology with XRCC4 and XLF. While XRCC4 and XLF are conserved in all eukaryotes, PAXX is absent in most invertebrates and in yeast[10]. DNA-PKcs share a similar evolutionary distribution with PAXX[10, 12], and it is proposed that the two proteins have evolved to participate in resolving more complex breaks in higher eukaryotes. PAXX has the ability to bind strongly and directly to Ku in a DNA-dependent manner, but is not capable of direct association with XLF, XRCC4, or Lig4[10, 13]. These features of PAXX differ from XRCC4 and XLF, where the former can have a stable interaction with Lig4, and the latter interacts with both Ku and XRCC4[10]. PAXX is believed to promote assembly and/or stability of the NHEJ machinery by stabilizing Ku at DNA ends[5], whereas XLF promote ligation by interacting with the XRCC4-Lig4 complex[14].

PAXX share several features with XLF; both of these proteins have the ability to interact with Ku in a DNA-dependent manner and they both promote end-ligation. Genetic studies have shown that PAXX and XLF function in the same pathway upon DSBs resulting in many chemical modifications and/or DSBs with non-cohesive ends (*e.g.* IR-induced DSBs). In contrast, the two proteins function in parallel sub-pathways rather than the same pathway in the repair of simple DSBs *in vitro*. This might be explained by the need of a more stable protein scaffold to maintain the DNA alignment during end-processing and ligation of complex DSBs, compared to the scaffold needed for the repair of less complex breaks[10].

Previously published *Paxx* knockout mouse models show an increase in radiosensitivity[13, 15, 16], whereas *Xlf* knockout mouse models show a modest reduction in lymphoid cell count numbers in addition to being radiosensitive[17, 18]. Single knockout *Paxx* and *Xlf* mice are viable and show no overt phenotype, but a combined deficiency of PAXX and XLF results in growth defects, neuronal apoptosis, Severe Combined Immunodeficiency (SCID), and embryonic lethality[13, 15, 16] . In addition, *Paxx*$^{-/-}$*Xlf*$^{-/-}$ cell lines reveal an increased sensitivity to radiation than that of single knockouts alone[15]. These findings suggest important overlapping functions between PAXX and XLF during the repair of DSBs.

Both PAXX and XLF are required for end-ligation during V(D)J recombination in developing B and T cells (described in Section 1.2.4), although they are functionally redundant and can compensate for each other's absence[19, 20]. Even though the two proteins have redundant functions during V(D)J recombination, their mechanism of function is thought to be distinct. PAXX-deficiency has no measurable effect on CSR in mature B cells[20], whereas XLF-deficient lymphocytes have shown about 50% reduction in switching efficiency from immunoglobulin (Ig) M to IgG_1 and IgG_3[18]. Moreover, XLF has been shown to be redundant with several proteins involved in DNA repair, including Recombination Activating Gene 1 and 2 (RAG1/2) and Ataxia Telangiectasia-Mutated (ATM)[12, 21], whereas PAXX show no redundancy with either of these proteins[19]. ATM-inhibition in XLF-deficient cells results in end-ligation defects that cannot be rescued by the overexpression of PAXX[13], and *Xlf*$^{-/-}$ cells are more sensitive to IR compared to *Paxx*$^{-/-}$ cells[19]. These findings support distinct, although unknown, roles of XLF and PAXX during DNA repair.

Human patients with mutations in *XLF* suffer from (to a varying extent) immunodeficiency, microcephaly, growth delay, and radiosensitivity [22]. Like human patients, XLF-deficient mice are radiosensitive, but in contrast only have a modest reduction in lymphocytes, and develop normally[18]. No human patients with mutations in the *PAXX* gene have been reported. However, it has been demonstrated that PAXX is indeed important during the repair of IR- and chemically-induced DSBs in human, chicken, and murine cells[5, 10, 11].

1.2 Lymphocyte Development

All cells of the immune system are derived from hematopoietic stem cells (HSCs) in bone marrow. HSCs differentiate through a series of progenitor stages able to eventually become mature lymphocytes. Lymphocytes are a subtype of white blood cells that includes two key players of the adaptive immune response; B and T cells. Progenitor T cells migrate from bone marrow to the thymus to complete their maturation, whereas the majority of remaining cells in bone marrow become B cells[23]. B and T cells randomly recombine variable (*V*), diversity (*D*), and joining (*J*) gene segments to produce unique antigen receptor (*AgR*) genes. This process, known as V(D)J recombination, forms immunoglobulin (*Ig*) genes in B cells, and T cell receptor (*TCR*) genes in T cells. The basis of adaptive immunity lies within the generation of these unique antigen receptor genes through recombination processes[24]. Adaptive immunity involves receptor diversity and specificity, as well as immunological memory after encountering an antigen (Ag)[23].

1.2.1 B Cells

B cell development in bone marrow involves rearrangement of heavy-chain (H-chain) *V*, *D,* and *J* variable gene segments, as well as rearrangement of κ or λ light-chain (L-chain) *V* and *J* variable gene segments. If successfully rearranged, two H- and two L-chains together make up the B cell receptor (BCR)[23] (Figure 1.2). The V, D, and J segments of the BCR H-chain, along with V and J segments of the L-chain are referred to as the variable region of the BCR and is the site of antigen-recognition[23].

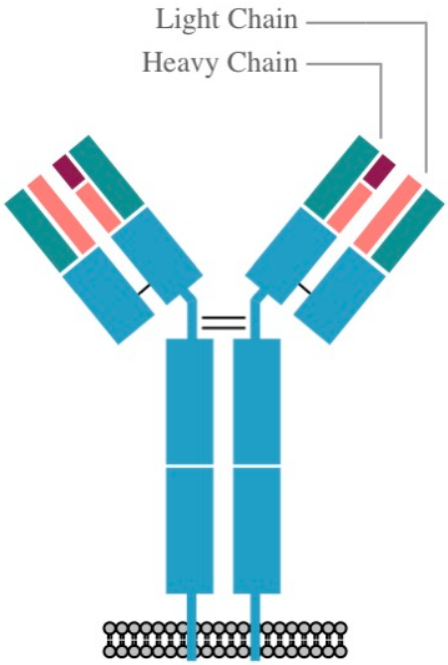

Figure 1.2: The B cell receptor, also called IgM due to H-chain mu (μ) constant regions, is composed of two H-chains and two L-chains (either κ or λ), consisting of variable and constant regions (H-chain μ constant regions). The constant regions of H- and L-chains are indicated in blue. The H-chain variable region have V (green), D (purple), and J (orange) segments, whereas the L-chain variable region only has V and J segments. Figure based on Owen, J., J. Punt, and S. Standford, *Kuby Immunology* (p. 242). 2013: Freeman, W. H. & Company.

Rearrangement of the H- and L-chain variable regions to form a functional BCR occurs through several steps in three defined developmental stages; the pro-B, pre-B and immature B stage[25], presented in Figure 1.3.

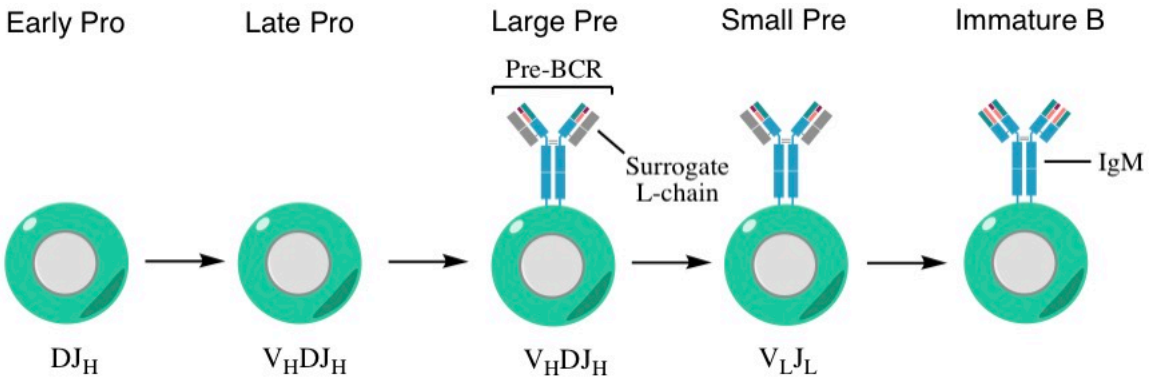

Figure 1.3: V(D)J recombination in developing B cells. At the pro-B cell stage, rearrangement of the H-chain D and J segments occurs (early pro), followed by V segment rearrangements at the late pro-B/large pre-B cell stage. If successfully rearranged, H-chains with μ constant regions and recombined variable regions are presented on the cell surface with surrogate L-chains to form the pre-BCR (large pre). Next, rearrangement of the L-chain V and J segments takes place (small pre). Successfully rearranged L-chains replace the surrogate L-chains of the pre-BCR, forming IgM (Immature B)[25]. Figure based on Owen, J., J. Punt, and S. Standford, *Kuby Immunology* (p. 340). 2013: Freeman, W. H. & Company.

Developing B cells undergo positive and negative selection processes to prevent un-responsive and self-reactive B cells from further development and proliferation[26]. Newly generated B cells with a functional BCR (also called IgM due to a H-chain mu constant region) are referred to as immature B cells. The expression of IgM on the B cell surface changes the expression pattern of many genes, ultimately leading to the migration of immature B cells from bone marrow to secondary lymphoid organs (*e.g.* spleen), where they can complete their differentiation into mature B cells. Activation of B cells upon encountering an Ag can trigger somatic hypermutation (SHM) of H- and L-chain variable regions and CSR of H-chain constant regions. SHM results in altered receptor affinity and specificity, whereas CSR leads to a change in isotype by switching expression from the mu constant region to a downstream constant region of the H-chain (IgM to IgG, IgA or IgE[E]). Specific isotypes have distinct effector functions, and the isotype switch depends on how the Ag is encountered, and the stimulatory signals received by the B cell[25].

[E] IgM, μ constant region. IgG, γ constant region. IgA, α constant region. IgE, ε constant region

B cells express distinct receptors depending on their developmental stage and linage commitment, making it possible to identify specific B cell subsets in a population of cells. The expression of CD43 (progenitor B cell marker), B220 (co-receptor), and IgM (BCR) on the cell surface can be used to distinguish between pro-, pre-, and immature B cells in bone marrow[13, 27] (Table 1.1). Another B cell marker frequently used is CD19, a co-receptor expressed on pro-, pre-, immature, and most mature B cells. However, terminally differentiated plasma B cells do not express CD19[28].

Table 1.1: Expression of CD43, B220, and IgM during pro-, pre-, and immature B cell developmental stages.

Developmental stage	**CD43**	**B220**	**IgM**
Pro-B	✓	✓	-
Pre-B	-	✓	-
Immature B	-	✓	✓

1.2.2 T Cells

Like B cells, T cells originate from HSCs in bone marrow, but in contrast to B cells mature in the thymus. T cell progenitors migrate from bone marrow to the thymus where they undergo several maturation steps to eventually become mature T cells. The T cell receptor can either be composed of a γ and a δ receptor chain, or an α and a β receptor chain**.** The majority of T cells express the TCRαβ, but approximately 5% express the TCRγδ. In addition to constant regions, the β and δ chains are composed of V, D, and J variable regions, whereas the α and γ chains are composed of V and J variable regions[23]. The T cell receptor αβ is presented in Figure 1.4.

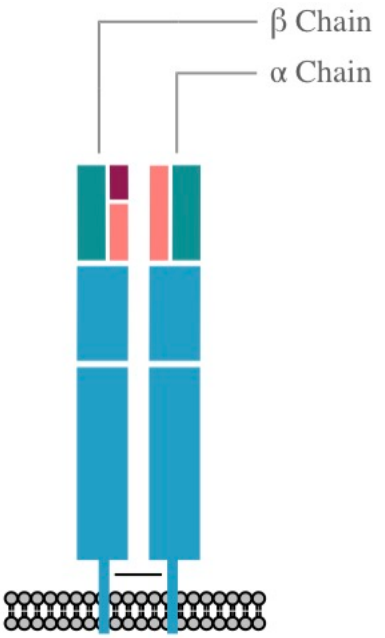

Figure 1.4: The T cell receptor αβ. The TCRαβ is composed of a β chain with V (green), D (purple), and J (orange) variable segments, and a α chain with V and J variable segments. Constant regions of the α and β chains are indicated in blue. Figure based on Janeway CA Jr, T.P., Walport M, *et al.*, *The Immune System in Health and Disease*, in *T cell receptor gene rearrangement*. 2001, Garland Science.

T cell-activation through the TCRαβ is dependent on co-receptors in the form of either CD4 or CD8, and CD3. The latter is a protein complex comprised of three dimers (CD3εγ, CD3εδ, and CD3ζζ)[30] that are important in signal transduction and Ag recognition. Whether a T cell express CD4 or CD8 determines the effector function of the T cell. CD4-expressing ($CD4^+$) cells are committed to the T helper (T_H) linage, and the CD8-expressing ($CD8^+$) cells are committed to the T cytotoxic (T_C) linage. The main effector function of T_H cells is to activate B cells and other cells of the immune system, whereas T_C cells mediate lysis of infected target cells. Most thymocytes develop into TCRαβ $CD4^+$ or $CD8^+$, but some thymocytes develop into other T cell lineages**.** Thymocytes lacking the expression of both CD4 and CD8 in the early developmental stages are referred to as double negative (DN, $CD4^-CD8^-$) cells, and the DN

phase is divided into four stages (DN1-DN4). Similar to B cells, T cells rearrange their receptor gene segments to produce functional TCRs. The rearrangement of *V, D,* and *J* gene segments of the β-chain locus occurs at the DN2 stage, and if successfully rearranged, the β receptor chain is paired and presented with a surrogate α chain on the T cell surface. The β-pre-α receptor assembles with CD3 complex proteins, which together make up the pre-TCR (DN3 stage). Rearrangement of the α chain locus (*V* and *J* gene segments) is initiated at the DN4 stage and completed at the double positive (DP, $CD4^+CD8^+$) stage. A successfully rearranged α receptor chain replaces the surrogate α chain, forming the TCRαβ (Figure 1.5). From here, T cells undergo positive and negative selection processes to ensure that only fitted T cells proceed. Depending on different cell interactions during the positive selection process, DP T cells mature into SP T cells, expressing either CD4 (T_H) or CD8 (T_C). T_H and T_C cells that pass the negative selection process are eventually ready to exit the thymus[23].

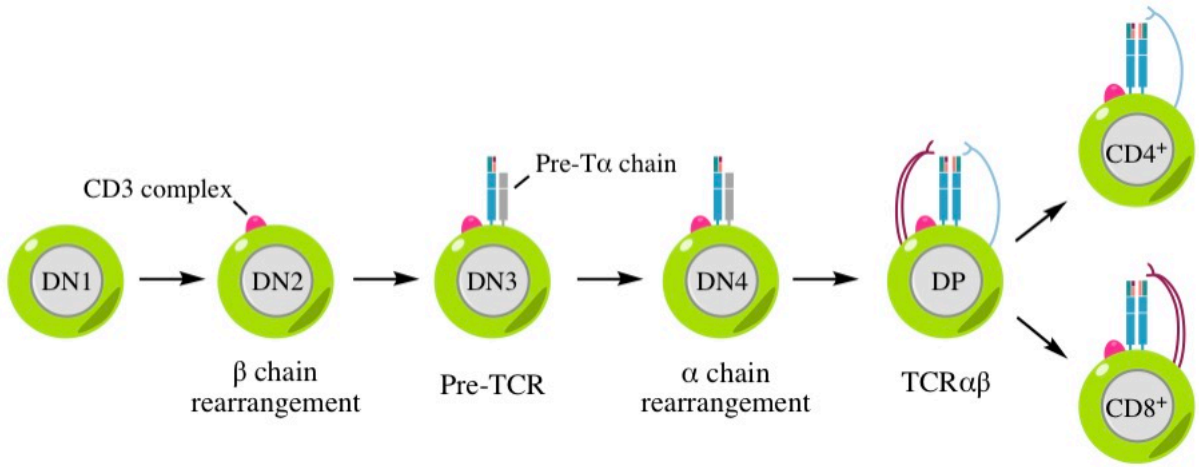

Figure 1.5: V(D)J recombination of the α and β receptor chains to form the TCRαβ in T cells. T cell precursors from bone marrow migrate to the thymus as DN1 cells, maturing into DN2 cells once they encounter and take residence in the thymic environment. During this stage, rearrangement of the β receptor chain begins. At the DN3 stage, a successfully rearranged β receptor chain is presented on the cell surface with a surrogate α chain. The β-Pre-α chains then associates with CD3 complex proteins, forming the pre-TCR. During the DN4 stage, the TCR α chain locus starts to rearrange. A successfully rearranged α chain replace the surrogate α chain, and the cells starts expressing CD4 and CD8 co-receptors, reaching the double positive (DP) stage. T cells then undergo positive and negative selection processes, eventually maturing into single positive (SP) $CD4^+$ or $CD8^+$ T cells. Figure based on Owen, J., J. Punt, and S. Standford, *Kuby Immunology* (p. 300). 2013: Freeman, W. H. & Company.

1.2.3 Lymphoid Cell Frequencies

The development of lymphocytes occurs in primary lymphoid organs (bone marrow and thymus), whereas the initiation of immune responses occurs in secondary lymphoid organs (*e.g.* spleen). The spleen specializes in capturing blood-borne antigens and removing old/damaged red blood cells (RBCs) by filtering circulating blood[31]. Excluding RBCs, the majority of splenocytes are B, T_H, and T_C cells. However, subpopulations of other immune cells such as distinct T cell linages, monocytes, granulocytes, dendritic cells, and natural killer cells are also found in the spleen[32]. Expected B and T cell frequencies in the murine spleen and thymus are provided in Table 1.2.

Table 1.2: Expected B and T cell frequencies (%) in the murine spleen and thymus**.** Table based on *Bio-Rad*. Flow Cytometry - Cell Frequency. 2017[32].

Spleen		**Thymus**	
Cell type	**Percent (%)**	**Cell type**	**Percent (%)**
T cells	21-35	$CD4^+$	4-6
$CD4^+$	13-20	$CD8^+$	1-2
$CD8^+$	7-15	$CD4^+CD8^+$	85-95
B cells	44-58	-	-

1.2.4 Mechanism of V(D)J Recombination

V(D)J recombination (Figure 1.6) is initiated in the G_1 phase of the cell cycle by the lymphocyte-specific proteins RAG1 and RAG2 (together referred to as RAG1/2) which induces DSBs adjacent to *V, D,* and *J* segments[24]**.** RAG1/2 recognizes specific DNA sequence motifs called Recombination Signal Sequences (RSSs) flanking *V, D,* and *J* segments**.** RSSs consist of three elements; a conserved 7bp sequence, a less conserved spacer of 12bp or 23bp, and a second conserved 9bp sequence. RAG1/2 strongly favors joining of a 12bp spacer with a 23bp spacer, ensuring that the joining of segments occur in the correct order**.** RAG1/2 introduces a single-strand nick between the segments being joined and their flanking RSSs[23]. Through several steps, this ultimately results in the generation of four broken ends; two blunt ends (signal ends) terminating in the RSS, and two closed hairpin formations (coding ends)[33]. Signal and coding ends are stabilized by RAG1/2 and other proteins (*e.g.* ATM), together referred to as the post-cleavage complex (PCC)[34]. Hairpins of coding ends are cleaved by the nuclease Artemis, and the resulting breaks are then processed and joined by the NHEJ machinery to form the coding joint. Formation of the coding joint often results in loss of nucleotides (through exonuclease activities) and non-templated addition of nucleotides by the Terminal deoxynucleotidyl Transferase (TdT); adding junctional diversity to the variable region of the receptor. Joining of signal ends is also mediated by NHEJ, forming the signal joint. Unlike coding joint formation, joining of signal ends usually do not require processing[24].

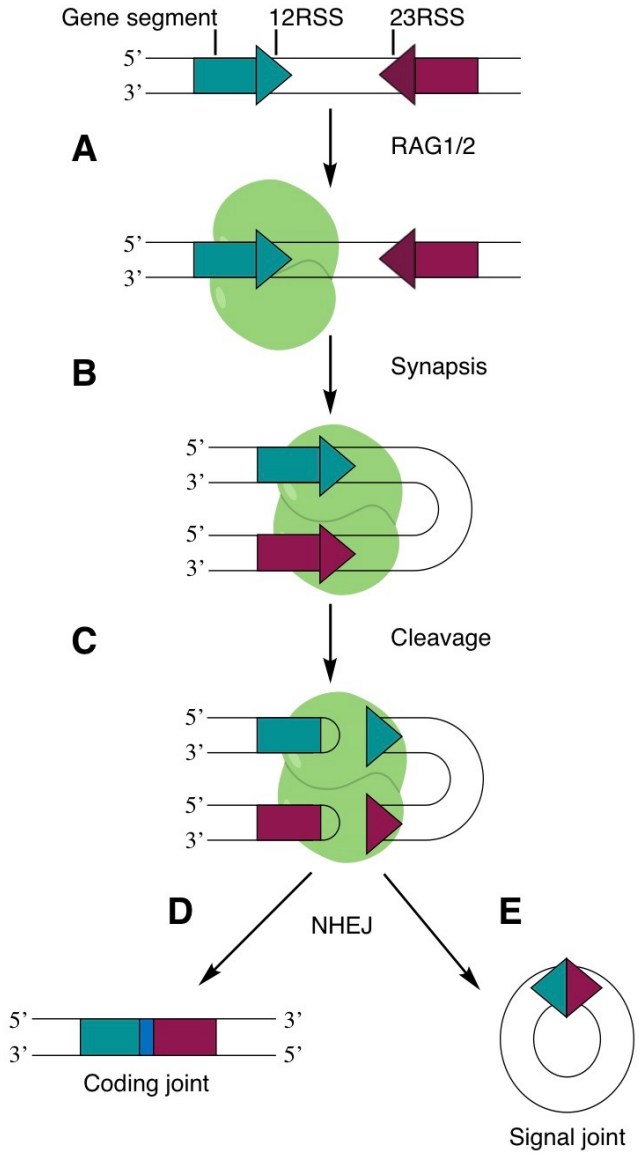

Figure 1.6: A simplified mechanism of V(D)J recombination. **A)** Antigen receptor gene segments flanked by a 12RSS or a 23RSS are recognized and bound by RAG1/2. **B)** Synapsis and nicking of RSSs adjacent to segments being joined by RAG proteins. **C)** Double strand cleavage and hairpin formation of coding ends. **D)** Hairpin opening by Artemis, end-processing, and end-joining by NHEJ factors. Processing of ends often results in nucleotide loss and addition (represented in blue). **E)** NHEJ of signal ends, forming the signal joint. Figure based on Schatz, D.G. and Y. Ji, *Recombination centres and the orchestration of V(D)J recombination*. Nat Rev Immunol, 2011. **11**(4): p. 255.

1.2.5 DNA Double-Strand Breaks and p53 Signaling

The assembly of B and T cell AgRs through V(D)J recombination is essential for adaptive immunity, but also holds a risk for autoimmunity through self-reactive AgRs and cancer development through *AgR* translocations. To prevent such adverse effects, the rearrangement process is strictly regulated[24]. The tumor suppressor p53 is a key protein in maintaining genomic stability by signaling appropriate responses to altered DNA structure (*e.g.* DSBs) and abnormal cellular metabolism. Through different DNA damage response (DDR) pathways, p53 can mediate cell cycle arrest, apoptosis, or senescence; thereby preventing uncontrolled proliferation of DNA damaged cells[35]. Upon DSBs, including those induced by RAG1/2 during V(D)J recombination, the ATM-dependent DDR is activated. ATM phosphorylates a variety of downstream factors mediating DNA repair and response to DNA damage, including p53. ATM phosphorylation of p53 upon DSBs promotes activation of the G_1/S checkpoints of the cell cycle, causing temporal cell cycle arrest. The cells able to repair their DSBs may proceed to the replicative stage of the cell cycle (S phase), whereas the cells with persistent DNA damage undergo apoptosis mediated through p53 signaling[36].

Mice deficient in NHEJ factors Lig4 or XRCC4, and double deficient XLF/DNA-PKcs mice are radiosensitive and have a SCID phenotype due to a block in early stages of B and T cell development[37, 38]. Moreover, Lig4- and XRCC4-deficient mice suffer from extensive neuronal apoptosis, resulting in embryonic lethality[38]. Double deficient XLF/DNA-PKcs mice have shown to be born at sub-Mendelian rations, but no pups survived past postnatal day 10[37]. The inactivation of p53 has been shown to rescue the lethality of these NHEJ-deficiencies[39-41], highlighting the interaction between p53 and NHEJ during growth and development.

1.3 NHEJ Deficiencies

Defective NHEJ as a consequence of mutated NHEJ genes leads to increased levels of radiosensitivity and may confer SCID. The severity of radiosensitivity and immunodeficiency varies, depending on both the gene mutated and the type of mutation. In the most severe cases, where V(D)J recombination is abolished, adaptive immunity is lost due to a block in early stages of B and T cell development[22]. Human patients with mutations in *LIG4*[42, 43], *XLF*[9], *ARTEMIS*[44], *DNA-PKcs*[45, 46], and *XRCC4*[47] have been identified, but patients with mutations in *PAXX, KU70,* or *KU80* has not been reported. Most mutations observed in humans are not fully inactivating, allowing residual protein function. Patients carrying mutated NHEJ genes may also suffer from varying degrees of microcephaly, growth defects and developmental delay, and are susceptible to cancer due to genomic instability. The phenotypic spectrum observed in patients reflects the importance of NHEJ to support normal growth and development in humans[22].

2 Objectives

Four *Paxx* mouse models[13, 15, 16, 48], including ours, have been published. In two of them, the full-length gene encoding PAXX was deleted[13, 16], whereas the third mouse model gained a *Paxx* frameshift mutation through CRISPR/Cas9 mutagenesis[15]. Our mouse model[48] only has a partial deletion of *Paxx* (still resulting in a null allele), preventing disruption of overlapping genes and genes in close approximation to *Paxx*; in particular *Clic3* (encoding chloride intracellular channel 3) which overlaps with *Paxx* in anti-sense orientation. Our mouse model is thus distinct from other *Paxx* mouse models previously described. **The first aim of this project** is to investigate the impact of *Paxx*-inactivation on growth and immune system development in our *Paxx* mouse model. This will be done by comparing the lymphoid cell counts, spleen weight, thymus weight, and body weight of our $Paxx^{+/-}$ and $Paxx^{-/-}$ mice to WT and NHEJ-defective mice. To determine the impact of *Paxx*-inactivation on lymphocyte development, B and T cell frequencies in spleen and thymus of PAXX-deficient mice will be compared to PAXX-proficient mice. The protein expression in spleen and thymus will also be investigated.

Single knockout *Paxx* and *Xlf* mice are viable and show no overt phenotype, but a combined deficiency results in embryonic lethality due to extensive apoptosis in the central nervous system[13, 15, 16]. The fact that these mice die as embryos, complicates the possibility to study the double-deficiency *in vivo*. The lethality of $Xrcc4^{-/-}$[40], $Lig4^{-/-}$[41], and double-deficient $Xlf^{-/-}DNA\text{-}PKcs^{-/-}$[39] mice is rescued by the inactivation of one or two alleles of *Trp53,* encoding p53. Based on phenotypic similarities among these deficient mice and $Paxx^{-/-}Xlf^{-/-}$ mice, it is proposed that p53-inactivation can rescue the lethality of double-deficient PAXX and XLF mice. **The second aim of this project** is to investigate if the lethality of $Paxx^{-/-}Xlf^{-/-}$ mice can be rescued by inactivating one or two alleles of *Trp53*, which will allow studying PAXX and XLF double-deficiency *in vivo.*

3 Materials and Methods

3.1 Mouse Models

Our *Paxx* mouse model was generated through a CRISPR/Cas9 gene editing approach in 2016 by genOway© (Lyon, France) upon request from the Oksenych group (IKOM, Faculty of Medicine and Health Sciences, NTNU, Norway)[48]. One sgRNA (#1) was designed to target the promoter region of *Paxx*; CCC AAG GGC TTG TAC TGC, and a second sgRNA (#2) was designed to target exon 1c in *Paxx*; GGC GGC GTC CGT CAC ACT in black6 mice (Figure 3.1.)

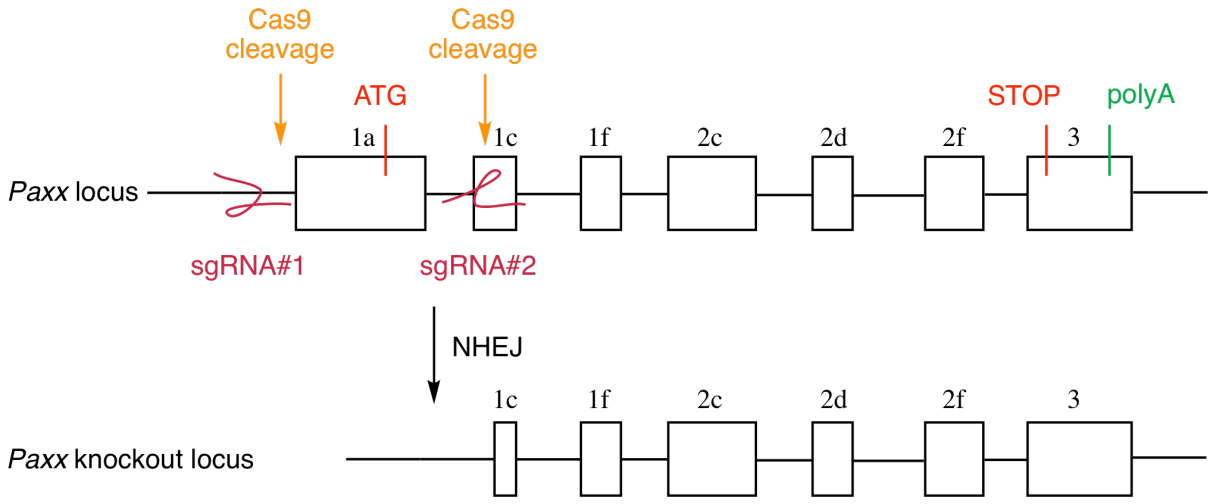

Figure 3.1: Schematic presentation of the original (top) and knockout (bottom) *Paxx* locus, indicating recognition sites by sgRNAs and cleavage sites by Cas9. Figure based on Gago-Fuentes, R., *et al.*, *Normal development of mice lacking PAXX, the paralogue of XRCC4 and XLF*. FEBS Open Bio, 2018. **8**(3).

A bioinformatics study performed by genOway© showed that *Paxx* overlaps with another gene in anti-sense orientation; *Clic3*, and the sgRNAs were thus carefully designed to avoid disruption of this additional gene. The two sgRNAs along with Cas9 RNA were microinjected into 158 zygotes collected from superovulated mice, and the treated zygotes were cultivated overnight before re-implantation into pseudopregnant foster mothers. This led to a total of 60 viable pups with a modified *Paxx* locus. Three independent mouse sub-strains with deletions of 636, 653, and 670bp in *Paxx* were provided by genOway (Table 3.1).

Table 3.1: Deletion details for the three heterozygous mutant lines obtained by back-crossing mutant founder mice with WT mice. The deletions range from 636-670 bp, yielding Polymerase Chain Reaction (PCR)-products ranging from 295-329 bp. Table based on Gago-Fuentes, R., *et al*., *Normal development of mice lacking PAXX, the paralogue of XRCC4 and XLF*. FEBS Open Bio, 2018. **8**(3).

Mutant line	Size of deletion (bp)	PCR-product (bp)	Deletion details
1	636	329	254bp of the promoter region, exon 1a and intron, and 3bp of exon 1c
2	653	312	Promoter region, exon 1a and intron, and 9bp of exon 1c
3	670	295	Promoter region, exon 1 and intron, and 27bp of exon 1c

Genetic modifications were verified by DNA sequencing and Polymerase Chain Reactions (PCRs). To develop a genotyping PCR assay, two oligonucleotide primers were designed to detect either the original *Paxx* locus (965 bp) or a significantly shortened modified locus corresponding to mutant alleles (329, 312, or 295bp). The primers used to identify mutant mice were designed to flank the regions targeted by the sgRNAs and Cas9; upstream of the promotor region and downstream of exon 1c (Figure 3.2).

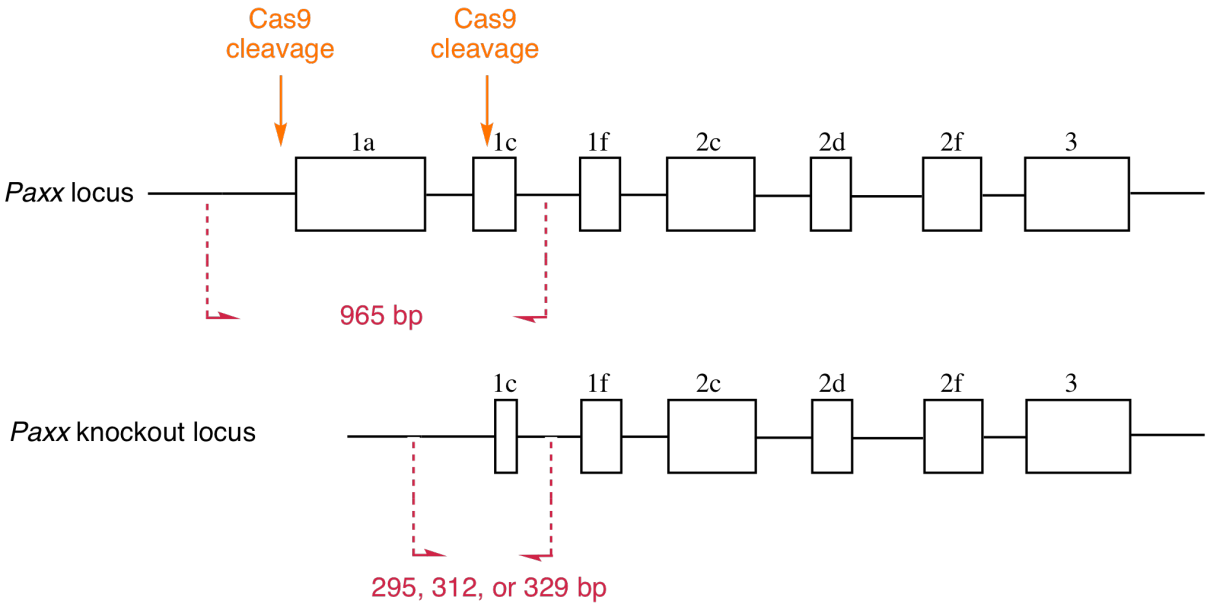

Figure 3.2: Schematic presentation of the WT and mutant alleles of *Paxx*. Dashed lines (red) indicate the hybridization sites for primers (forward/reverse), as well as expected PCR-products. Site of Cas9 cleavage indicated (orange). Figure based on Gago-Fuentes, R., *et al*., *Normal development of mice lacking PAXX, the paralogue of XRCC4 and XLF*. FEBS Open Bio, 2018. **8**(3).

Other mouse models used in this project have previously been described; *Xlf*[18], *DNA-PKcs*[49], *Ku80*[50], *Trp53*[51], and *Scid*[52]. The *Scid* mouse model is a natural mutant mouse with a nonsense mutation in the gene encoding DNA-PKcs, resulting in a SCID phenotype[52, 53]. *Scid*$^{-/-}$ mice were initially planned as NHEJ-defective controls for experiments, but DNA-PKcs and Ku80 deficient mice were chosen instead due to availability. All experiments involving mice were performed according to protocols approved by the Norwegian University of Science and Technology (NTNU). Primer sequences for genotyping and expected amplicons are provided in Appendix A, p. I.

3.2 Genotyping

3.2.1 DNA Extraction from Tissue and the Polymerase Chain Reaction

Ear-samples from mice were incubated overnight at 56°C with Proteinase K Solution diluted from 50x stock (Invitrogen™, Carlsbad, California, USA) and DNA lysis buffer (10mM Tris pH9.0, 1M KCl, 0.4% NP-40, 0.1% Tween 20) to extract DNA. The samples were incubated at 95°C for 30 minutes the next day. Debris was spun down at 15 000g for 10 minutes, and the DNA concentration was measured by a Nanodrop® ND-1000 Spectophotometer (Thermo Scientific, Waltham, Massachusetts, USA). Samples where diluted to get a final DNA concentration of ~50ng/µL. The PCRs were performed with ~50ng DNA in a final reaction volume of 25µL, using the Taq 2x Master Mix Kit (New England Biolabs® Inc., Ipswich, Massachusetts, USA). PCRs were run in a 2720 Thermal Cycler (Applied Biosystems™, Foster City, California, USA)**.** PCR programs are provided in Appendix B, p. III.

3.2.2 Electrophoresis

Agarose gels with GelRed™ Nucleic Acid Gel Stain (diluted from 10 000x stock**,** Biotium, Fermont, California, USA) were prepared from 1% SeaKem® LE Agarose (Lonza, Basel, Switzerland) in Tris-Borate-EDTA (TBE) buffer (pH 8.4; 89mM Tris; 89mM Boric Acid; 2mM EDTA). Gel electrophoresis was performed in TBE buffer at 130V for 70 minutes (100mL gels) or 135 minutes (300mL gels)**,** and the sample volume loaded was 10µL (~20ng DNA). For reliability, both positive and negative controls were used in all assays. Quick-Load® 100bp DNA Ladder (New England Biolabs® Inc.) and Orange G 5x ~50bp (15% glycerol; 0.2% Orange G dye, dH_2O) were used as ladder and tracking dyes, respectively. The gels were visualized and pictured with a ChemiDoc™ MP Imaging System (Bio-Rad, Hercules, California, USA).

3.3 Cell Count in Lymphoid Organs

The spleen, thymus and femurs were isolated from mice and collected in petri dishes with 5 mL of Phosphate-Buffered Saline (PBS). For spleen and thymus, the plunger of a syringe was used to mash the tissue to release cells into the PBS solution. A syringe with a BD Microlance™ 0.8 x 40mm needle was used to flush PBS through the medullary cavity of femurs to isolate bone marrow. The cell suspensions were filtrated into 50mL conical centrifuge tubes through 40 μm Fisherbrand™ Sterile Cell Strainers (Fisher Scientific, Hampton, New Hampshire, USA) and spun down at 1500 rpm for 5 minutes (4°C). Pellets were gently resuspended in 1mL of Red Blood Cell Lysis Buffer Hybri-Max™ **(**Sigma-Aldrich, St. Louis, Missouri, USA**)** and left for 5 minutes to lyse RBCs. Cells were diluted with PBS to a final volume of 14mL**.** The cells were counted in Countess II FL Automated Cell Counter (Invitrogen™) using Trypan Blue Stain 0.4% (Invitrogen™) and Countess™ Cell Counting Chamber Slides (Invitrogen™).

3.4 Protein Extraction from Tissue and Calculation of Concentration

Samples from spleen and thymus (~20 mg) were collected in 2mL Precellys® Lysing Tubes (Bertin Technologies, Versailles, France) with 5-10 Precellys® 1,4mm Zirconium Oxide Beads (Bertin Technologies), and 200µL of RIPA lysis buffer (10mM Tris pH8, 1% Triton, 0.1% SDS, 150mM NaCl, 1mM EDTA, 20mM Sodium pyrophosphate pH7.2, Pefabloc diluted from 1000x stock (Sigma-Aldrich), Phosphatase Inhibitor Cocktail 2 diluted from 100x stock (Sigma-Aldrich), Protease Inhibitor Cocktail diluted from 25x stock (Sigma-Aldrich))**.** Samples were homogenized in a MagNA Lyser (Roche, Basel, Switzerland) at 5000 rpms for 10 seconds before a 20-minute centrifugation at 15 000g, 4°C. Supernatants were collected in microcentrifuge tubes, and the protein concentration was determined by a Bradford assay, using Protein Assay Dye Reagent (Bio-Rad). The absorbance was measured at 595nm in a UV-1700 Spectrophotometer (Shimadzu, Kyoto, Japan), from which the final protein concentration was calculated, based on a Bovine Serum Albumin (BSA) standard curve. Preparation of BSA standards and measured absorbance is presented in Table 3.2 and 3.3, respectively. The BSA standard curve is presented in Figure 3.3.

Table 3.2: Preparation of BSA standards. A BSA standard curve was prepared for determining the concentration of protein extracts from tissue by performing a Bradford assay. The Protein Assay Dye Reagent was diluted five times in dH_2O prior to measurements. A stock solution of BSA (2µg/µL) was used.

	Standards					
	1	**2**	**3**	**4**	**5**	**6**
BSA (µg)/sample	0	2	4	10	14	22
Stock BSA (µL)	0	1	2	5	7	11
H_2O (µL)	20	19	18	15	13	9
5x diluted Protein Assay Dye Reagent (µL)	1000					

Table 3.3: Measured absorbance of BSA standards. The absorbance was measured at 595nm for prepared 0, 2, 4, 10, 14, and 22µg BSA standards. The plot is presented in Figure 3.3.

	Standards					
BSA (µg)	0	2	4	10	14	22
A_{595nm}	0.003	0.131	0.216	0.443	0.727	0.970

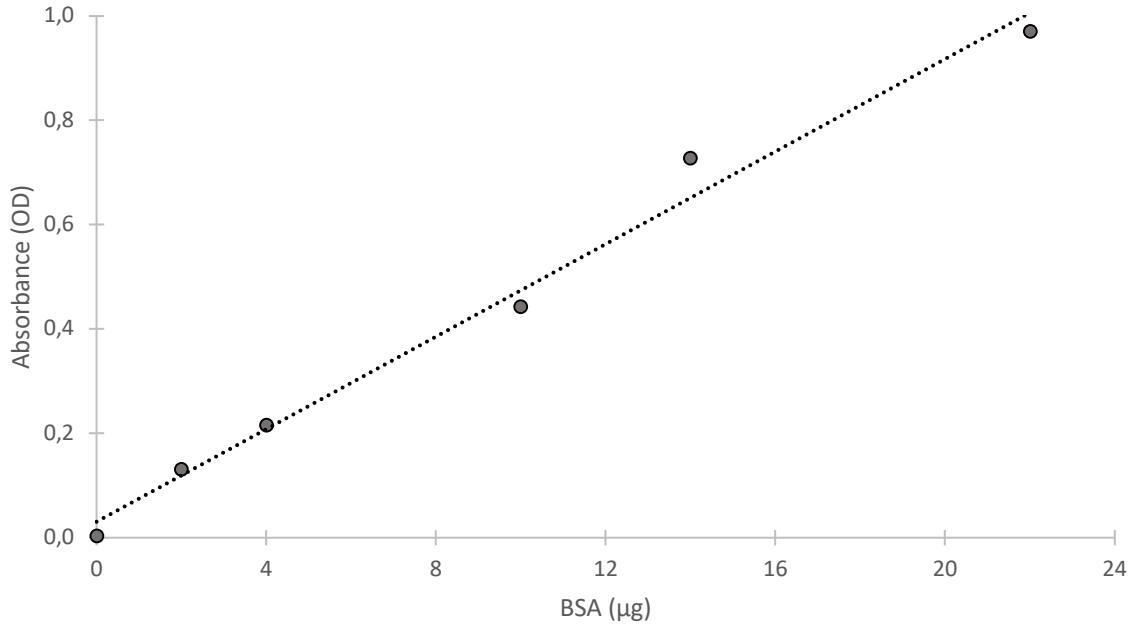

Figure 3.3: BSA standard curve. A BSA standard curve was prepared for determining the protein concentration of whole cell lysates from tissue by performing a Bradford assay. The equation, $y = 0.044x + 0.031$, $R^2 = 0.987$, was used to estimate the protein concentration in cell lysates from organs.

For determination of protein concentration in whole cell lysates from organs, 19µL dH_2O, 1µL of sample, and 1000µL Protein Assay Dye Reagent (diluted 5x in dH_2O) was mixed prior to absorbance measurements. The final protein concentration was calculated from the BSA standard curve.

3.5 Western Blot

3.5.1 Electrophoresis

Protein samples (~80 μg) for western blot analysis were prepared using NuPAGE® LDS Sample Buffer (originally 4x stock) and 0.1M DTT (Thermo Scientific) following a 10-minute incubation at 70°C. The samples were run in NuPAGE™ 10% Bis-Tris gels (Thermo Fisher Scientific, Waltham, Massachusetts, USA) at 160V for 70 minutes in NuPAGE™ MOPS SDS Running Buffer (diluted from 20x stock,Thermo Fisher Scientific). MagicMark™ XP Western Protein Standard (Invitrogen™) and SeeBlue™ Pre-stained Protein Standard (Invitrogen™) was used for molecular weight estimation and tracking during electrophoresis.

3.5.2 Electroblotting

Wet electroblotting was run at 25V for 70 minutes in 10% Methanol NuPAGE™ Transfer Buffer (20x stock) with NuPAGE™ Antioxidant (1000x stock, Invitrogen™)**.** Amersham™ Hybond™ PDVF Blotting Membranes pore size 0.45μm (GE Healthcare Life Sciences, Marlborough, Massachusetts, USA) were used for protein transfer. Semi-dry electroblotting was run in a Trans-Blot® Turbo™ Transfer System (Bio-Rad) at 25V for 7 minutes using Trans-Blot® Turbo™ Mini Nitrocellulose (0.20μm) Transfer Packs (Bio-Rad).

3.5.3 Chemiluminescent Detection and Quantification

Membranes were blocked for 1h RT in 5% milk (Non-fat dry milk, PBS-T; 0.1% Tween 20) following overnight incubation at 4°C with the primary antibody diluted in 5% milk. Membranes were washed three times for 5 minutes with PBS-T following 1h incubation with Horseradish Peroxidase (HRP)-conjugated secondary antibodies diluted in 5% milk (RT). Membranes were washed again as previously described, prior to chemiluminescent protein detection with SuperSignal™ West Femto Maximum Sensitivity Substrate (Thermo Scientific) in a ChemiDoc™ MP Imaging System (Bio-Rad)**.** All incubations were done on a rocker. β-actin was used as loading control. Protein quantification of western blots was performed using the ImageJ software (U. S. National Institutes of Health, Maryland, USA). Antibodies used in western blots are described in Section 3.8.

3.6 Staining of Cells for Flow Cytometry

The murine spleen and thymus was isolated in petri dishes with cold PBS-5% Fetal Bovine Serum (FBS), thereafter being mashed, filtrated, and centrifuged as previously described (Section 3.3). Pellets were resuspended in 1 mL of Red Blood Cell lysing buffer Hybri-Max (Sigma-Aldrich) and incubated for 5 minutes at room temperature (RT, ~22°C). Cells were then washed with 10mL PBS-5% FBS and spun down. Pellets were resuspended in 10ml PBS-5% FBS and filtered through a 40µm cell strainer once more. Cells were counted as previously described (Section 3.3). The cell suspensions were spun down and diluted with PBS-2% FBS to get a final concentration of $2.5*10^6$/100µL. Each sample of $2.5*10^6$ cells were blocked for 15 minutes (RT) with Mouse BD Fc Block™ (BD Biosciences, New Jersey, USA) diluted 50x in PBS-2% FBS. Samples were then incubated with fluorochrome-conjugated antibodies diluted in PBS-2% FBS for 30 minutes in darkness, 4°C. The cells were washed and spun down (1500rpm, 5 minutes, 4°C) two times with 500µL PBS-2% FBS, before transfer intro Falcon™ Round-bottom polystyrene tubes (Corning™, New York, USA). Single-stained CD3/CD19/CD4/CD8 BD™ CompBead Anti-Rat and Anti-Hamster Ig κ particles (BD Biosciences) were used for compensation. Negative Control Compensation Particles (BD Biosciences) and unstained splenocytes/thymocytes were used as controls. The samples were run in a BD FACSCanto™ flow cytometer using the BD FACSDiva™ software, and the data was further analyzed using the FlowJo® software (FlowJo LLC). Antibodies used in flow cytometry are described in Section 3.8.

3.7 *Paxx.Xlf.Trp53* Breeding

Initially, our *Paxx* mouse model[48] was crossed with mice heterozygous for *Xlf*[18]. *Paxx*$^{+/-}$*Xlf*$^{+/-}$ mice were then crossed with *Trp53*$^{+/-}$ mice[51] to obtain suitable genotypes for further breeding. Later, *Paxx*$^{+/-}$*Xlf*$^{+/-}$*Trp53*$^{+/-}$ mice were crossed with each other, and *Paxx*$^{+/-}$*Xlf* $^{-/-}$*Trp53*$^{+/-}$ crossed with *Paxx*$^{+/-}$*Xlf*$^{+/-}$*Trp53*$^{+/-}$.

3.8 Antibodies

Information about antibodies used during western blotting and flow cytometry is presented in Table 3.4 and 3.5, respectively.

Table 3.4: Listed antibodies were used in western blots. The table indicates antibody host and target, dilutions used, reference (catalogue number), as well as the antibody supplier.

Antibody	Host and target, type	Dilution	Reference (Catalog #)	Supplier
Anti-PAXX	Rabbit Anti-Human, polyclonal	1:200	ab126353	Abcam, Cambridge, United Kingdom
Anti-XLF	Rabbit Anti-Human, polyclonal	1:2000	A300-730A	Bethyl Laboratories, Montgomery, Alabama, USA
Anti-p53	Mouse Anti-Human, monoclonal	1:500	MA5-12571	Invitrogen, Carlsbad, California, USA
Anti-p53	Mouse Anti-Human, monoclonal	1:500	sc-126	Santa Cruz Biotechnology, Dallas, Texas, USA
Anti-p53	Rabbit Anti-Human, polyclonal	1:1000	sc-6243	Santa Cruz Biotechnology
Anti-β-actin	Mouse Anti-Human, monoclonal	1:2000	ab8226	Abcam
Anti-Mouse (HRP-conjugated)	Rabbit Anti-Mouse, polyclonal	1:5000	P0260	Dako Agilent, Santa Clara, USA
Anti-Rabbit (HRP-conjugated)	Swine Anti-Rabbit, polyclonal	1:5000	P0399	Dako Agilent

Table 3.5: Listed antibodies were used in flow cytometry. The table indicates antibody fluorochrome conjugate, host and target, dilution used, reference (catalog number), and the antibody supplier. Given dilutions were used for $2.5*10^6$ cells.

Antibody	Fluorochrome Conjugate	Host and target, type	Dilution	Reference (Catalog #)	Supplier
Anti-CD16/CD32 (Fc Block)		Rat Anti-Mouse, monoclonal	1:50	553141	BD Biosciences, New Jersey, USA
Anti-CD3ε	APC	Hamster Anti-Mouse	1:100	100312	Biolegend, San Diego, California, USA
Anti-CD4	PE-Cy7	Rat Anti-Mouse, monoclonal	1:100	25-0042-81	Thermo Scientific, San Diego, California, USA
Anti-CD8α	PE-Cy5	Rat Anti-Mouse, monoclonal	1:100	553034	BDBiosciences
Anti-CD19	Pe-Cy7	Rat Anti-Mouse	1:100	115520	Biolegend

3.9 Statistics

Statistical analysis of cell counts, spleen weight, thymus weight, and body weight among genotypes were performed using GraphPad Prism 7 (La Jolla, California, USA). A one-way ANOVA was performed for all groups of variables. To compare proportions of B and T lymphocytes in PAXX-proficient and PAXX-deficient mice, unpaired t-tests were performed.

4 Results

4.1 Genotyping

Genotypes of mice for organ isolation, cell count, western blot analysis, flow cytometry, and breeding were verified by PCR and gel electrophoresis. DNA extracted from murine ear-samples were used.

Examples of all PCR assays performed during this project are presented in Figure 4.1; A) *Paxx* WT and mutant alleles, B) *Xlf* mutant allele, C) *Xlf* WT allele, D) *Trp53* WT and mutant alleles, E) *DNA-PKcs* WT allele, F) *DNA-PKcs* mutant allele, G) *Ku80* WT and mutant allele, and H) *Scid* WT and mutant allele. *Scid*$^{-/-}$ mice were initially planned as NHEJ-defective controls for experiments, but due to availability, the choice fell upon DNA-PKcs and Ku80 deficient mice instead. Positive, negative, and dH_2O controls were used in all PCR assays for reliability.

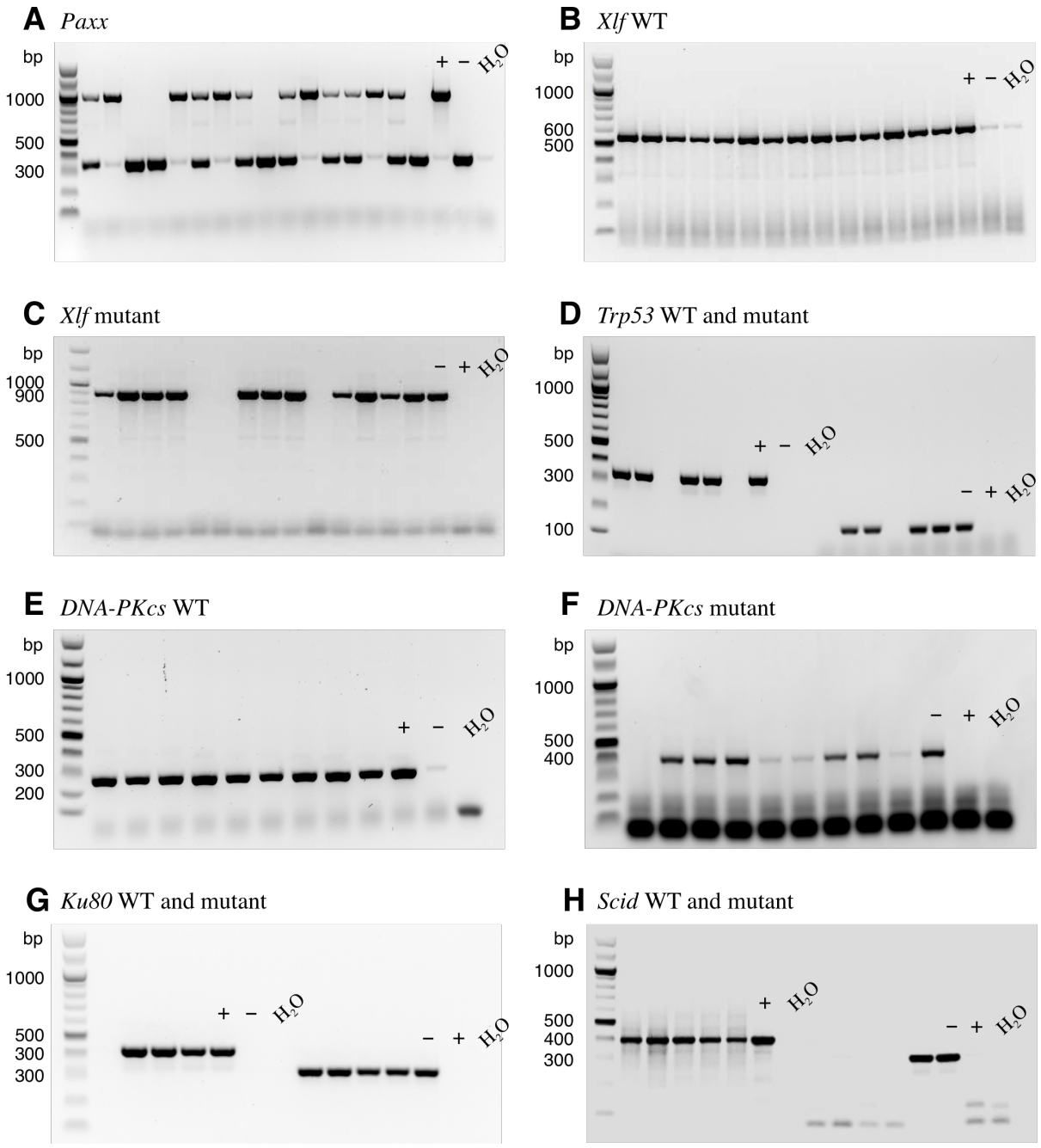

Figure 4.1: Examples of PCR analysis for *Paxx, Xlf, Trp53, DNA-PKcs*, *Ku80,* and *Scid* with indicated controls; "+" indicates WT, and "–" indicates double knockout. **A)** *Paxx.* The upper band correspond to the WT allele (965bp), whereas the lower band correspond to the mutant allele (either 329, 312, or 295bp). **B)** *Xlf* WT. Bands correspond to the *Xlf* WT allele (650bp). **C)** *Xlf* mutant. Bands correspond to the *Xlf* mutant allele (950bp). Samples with no band are homozygous for the WT allele. **D)** *Trp53* WT and mutant. Samples with an amplified WT allele (321bp) are shown to the left, and samples with an amplified mutant allele (150bp) are shown to the right. **E)** *DNA-PKcs* WT. Bands correspond to the WT allele (250bp). **F)** *DNA-PKcs* mutant. Bands correspond to the mutant allele (427bp). **G)** *Ku80* WT and mutant. Samples with an amplified WT allele (400bp) are shown to the left, and samples with an amplified mutant allele (320bp) are shown to the right. **H)** *Scid* WT and mutant. Samples with an amplified WT allele (409bp) are shown to the left, and samples with an amplified mutant allele (316bp) are shown to the right.

4.2 Growth and Immune System Development

The spleen, thymus, and body weight (n=38), as well as the cell count in spleen, thymus and femoral bone marrow (n=33) was recorded to detect any possible differences among WT, *Paxx*$^{+/-}$, *Paxx*$^{-/-}$, or *Xlf*$^{-/-}$ mice. DNA-PKcs- (n=4) and Ku80-deficient (n=3) mice were used as NHEJ-defective controls for all comparisons. Both DNA-PKcs- and Ku80-deficiency confers SCID in mice as a result of defective V(D)J recombination[22]. *Ku80*$^{-/-}$ mice also have a significantly reduced body weight compared to the WT, whereas *DNA-PKcs*$^{-/-}$ mice exhibit no additional phenotype other than SCID and a modest defect in DNA repair[22, 54]. Spleen and thymus development in WT, *Paxx*$^{+/-}$, *Paxx*$^{-/-}$, and *DNA-PKcs*$^{-/-}$ is presented in Figure 4.2, indicating the phenotypic effect of SCID in spleens and thymi of DNA-PKcs-deficient mice.

Males and females were pooled together for analysis, and mice were between 4-10 weeks of age. Average values and comparisons with indicated significance and related p-values are provided in Appendix C, p. V.

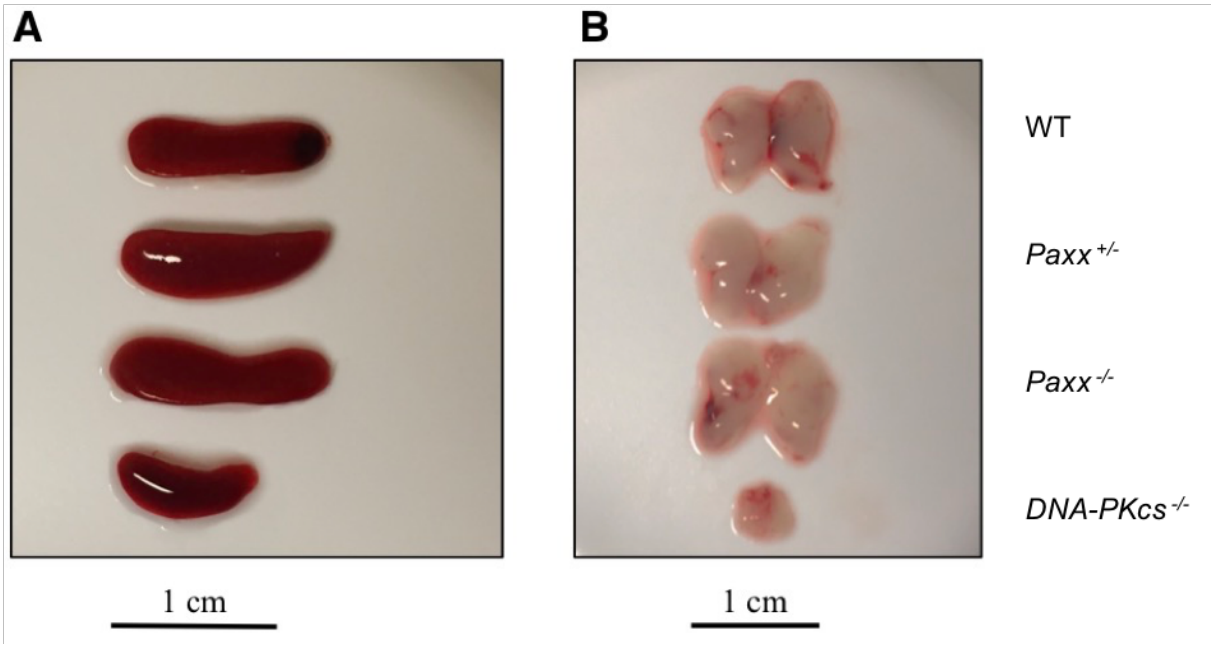

Figure 4.2: Development of spleen and thymus in WT, *Paxx*$^{+/-}$, *Paxx*$^{-/-}$, and *DNA-PKcs*$^{-/-}$ mice. **A)** Examples of spleens isolated from WT, *Paxx*$^{+/-}$, *Paxx*$^{-/-}$, and *DNA-PKcs*$^{-/-}$ mice. **B)** Examples of thymi isolated from WT, *Paxx*$^{+/-}$, *Paxx*$^{-/-}$, and *DNA-PKcs*$^{-/-}$ mice.

There was no significant difference in spleen weight among WT (n=8), *Paxx*$^{+/-}$ (n=14), *Paxx*$^{-/-}$ (n=11), and *Xlf*$^{-/-}$ (n=5) mice (Figure 4.3A). Both *Xlf*$^{-/-}$ and *Paxx*$^{-/-}$ mice had a significant reduction in splenocyte numbers (Figure 4.3B) compared to the WT (p=0.0003 and p=0.0041, respectively), but they were not significantly different from each other (p=0.5942). XLF-deficient mice also showed a significant reduction in number of splenocytes compared to *Paxx*$^{+/-}$ mice (p= 0.0053).

No significant difference in thymus weight or thymocyte count was observed among WT, *Paxx*$^{+/-}$, and *Paxx*$^{-/-}$ mice (Figure 4.3C and 4.3D, respectively). The thymocyte count in *Xlf*$^{-/-}$ mice was significantly reduced when compared to the WT (p=0.0026), which may reflect the observed reduction in thymus weight in *Xlf*$^{-/-}$ mice compared to WT mice (p=0.0106). The thymocyte count was also significantly reduced in *Xlf*$^{-/-}$ mice when compared to *Paxx*$^{+/-}$ mice (p=0.0261). Neither the thymus weight (p=0.0512) nor the thymocyte cell count (p=0.1372) in *Xlf*$^{-/-}$ mice was significantly different from *Paxx*$^{-/-}$ mice.

There was no significant difference in bone marrow cell counts among WT, *Paxx*$^{+/-}$, *Paxx*$^{-/-}$, *Xlf*$^{-/-}$, and *DNA-PKcs*$^{-/-}$ mice (Figure 4.3E). The cell count in *Ku80*$^{-/-}$ mice was significantly reduced when compared to WT, *Paxx*$^{+/-}$, and *Paxx*$^{-/-}$ mice (p=0.0048, p=0.0014, and p=0.0433, respectively).

WT, *Paxx*$^{+/-}$, *Paxx*$^{-/-}$, *Xlf*$^{-/-}$ and *DNA-PKcs*$^{-/-}$ mice had similar body weights (Figure 4.3F), whereas *Ku80*$^{-/-}$ mice showed a significant decrease in size compared to WT and *Paxx*$^{+/-}$ (p=0.0065, and p=0.0367, respectively).

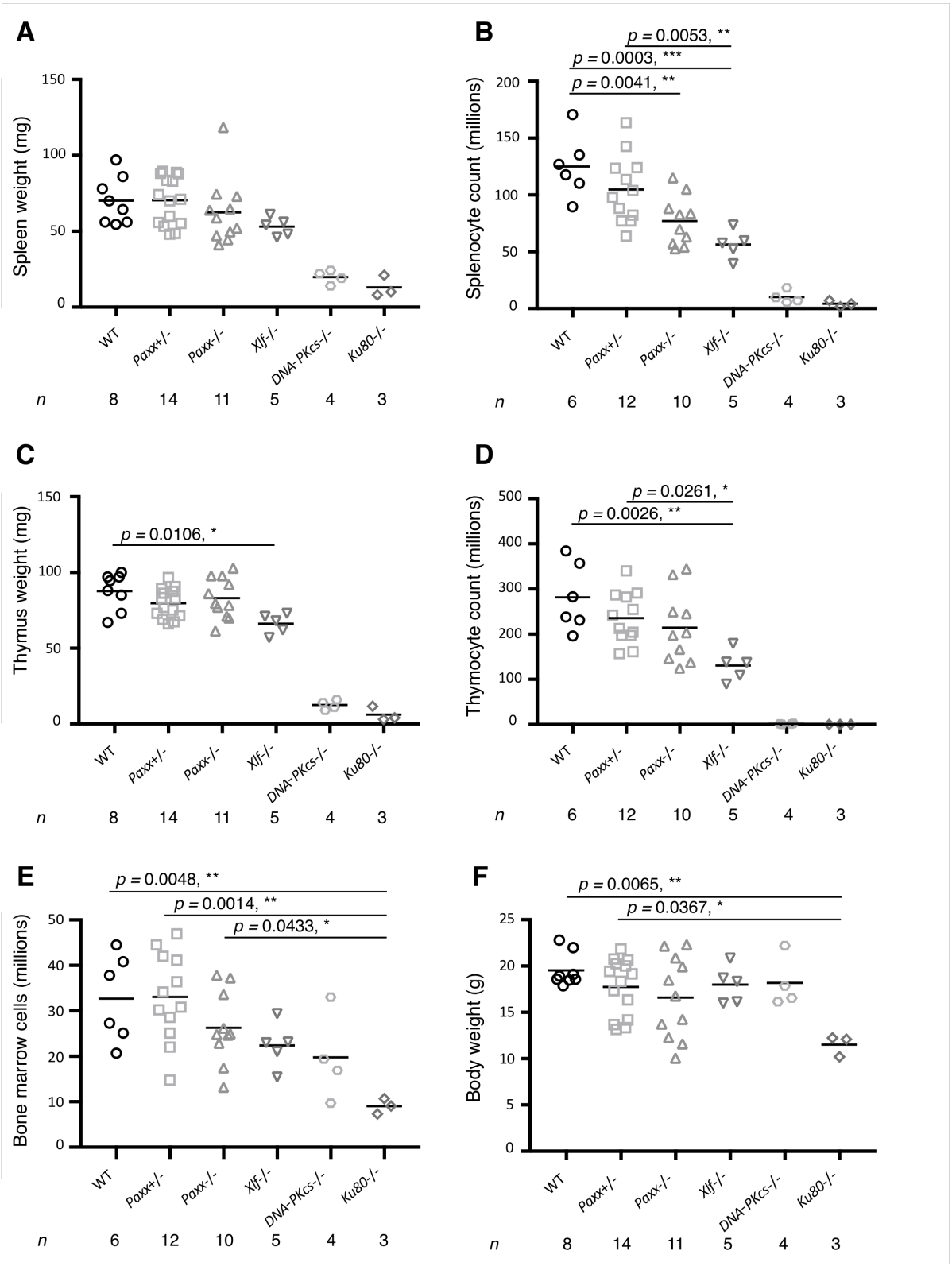

Figure 4.3: Comparisons in cell counts, spleen weight, thymus weight, and body weight among WT, *Paxx*$^{+/-}$, *Paxx*$^{-/-}$, and *Xlf*$^{-/-}$ mice. *DNA-PKcs*$^{-/-}$ and *Ku80*$^{-/-}$ mice were used as NHEJ-defective controls. Number (*n*) of each genotype analyzed is indicated. **A)** Weight (mg) of isolated spleens. **B)** Splenocyte count (millions) after RBC lysis. **C)** Weight (mg) of isolated thymi. **D)** Thymocyte count (millions) after RBC lysis. **E)** Cell count (millions) of femoral bone marrow after RBC lysis. **F)** Body weight (g) of mice.

4.3 Protein Expression in Lymphoid Organs

Whole cell protein extracts from spleens and thymi of *Paxx, Xlf,* and *Trp53* mice were used for investigating the protein expression among WT, heterozygous, and knockout mice. The intention was to analyze the expression of PAXX, XLF, and p53 in mice individually, to have these results ready if $Paxx^{-/-}Xlf^{-/-}Trp53^{+/-}$ or $Paxx^{-/-}Xlf^{-/-}Trp53^{-/-}$ mice proved to be viable. Three Anti-Human p53 antibodies were tested for cross-reactivity with murine p53 protein.

Paxx knockout was confirmed by the absence of PAXX (22kDa) protein in both spleen and thymus (Figure 4.4A). The heterozygous mouse showed a decrease in protein expression in both spleen and thymus when compared to the WT (45.1% and 31.6%, respectively). Protein quantification indicated that PAXX expression in the spleen was reduced by 52.5% when compared to PAXX expression in the thymus. A distinct PAXX blot with independent WT, heterozygous and knockout mice is presented in Appendix D, p. IX.

Knockout was confirmed by the absence of XLF protein in both spleen and thymus (Figure 4.4B). Reduction of XLF expression was observed in the $Xlf^{+/-}$ mouse in both spleen and thymus when compared to the WT (25.2% and 53.5% reduction, respectively). XLF expression in the WT spleen was reduced by 17.5% compared to the thymus, whereas PAXX expression varied more between WT organs (52.5% reduction in spleen). Western blots indicate that XLF is more abundantly expressed in the spleen compared to splenic PAXX expression.

Calculations are based on protein quantification of PAXX (Figure 4.5) and XLF (Figure 4.6) western blots, without subtracting background levels. The protein expression of PAXX and XLF was normalized by the loading control, β-actin. Genotypes of mice were verified by PCR two times with independent DNA samples.

Initially, two different Mouse Anti-Human p53 antibodies **(**Invitrogen; MA5-12571, and Santa Cruz; sc-126) were used to test for cross-reactivity with murine p53 (53kDa). For both antibodies, several bands were observed in all samples from both spleen and thymus (MA5-12571; Figure 4.4C**,** sc-126; Figure 4.4D), including the *Trp53*$^{-/-}$ control. To investigate whether bands around 50kDa were unspecific, an additional antibody was tested (Rabbit Anti-Human p53, Invitrogen; sc-6243) with splenic protein extracts from *Trp53*$^{+/+}$ and *Trp53*$^{-/-}$ mice along with Human HAP1[F] WT lysates as a positive control (Figure 4.4E). Here, bands observed using Mouse Anti-Human p53 antibodies were absent in both *Trp53*$^{+/+}$ and *Trp53*$^{-/-}$. Two bands around 45-50 kDa were observed in HAP1 WT cells, but no negative control (*e.g.* human *Trp53*$^{-/-}$ cells) were available at the time to verify that these bands were specific in human cells (Figure 4.4E). The same bands around 25 and 50kDa that were observed in blots using Mouse Anti-Human antibodies (Figure 4.4C and 4.4D) were also observed when detecting β-actin in splenic protein extracts from *Trp53*$^{+/+}$ and *Trp53*$^{-/-}$ mice (Figure 4.4F) using Mouse Anti-β-actin secondary antibody.

[F] Haploid human cell line (Horizon Discovery, Cambridge, United Kingdom)

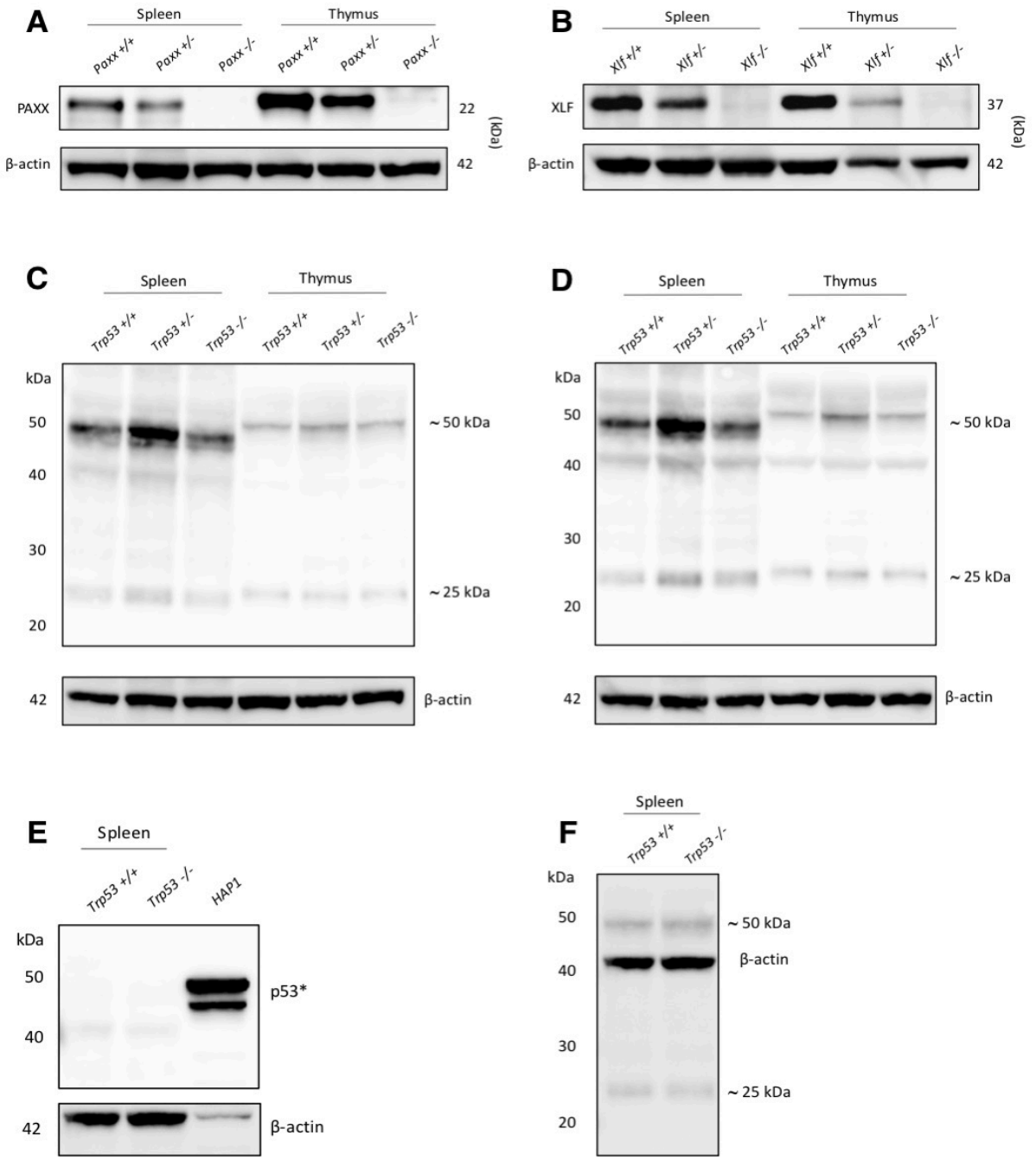

Figure 4.4: Western blots of PAXX (22kDa), XLF (37kDa), and p53 (53kDa) in WT, heterozygous, and knockout mice (80µg protein loaded). β-actin was used as loading control in all blots. **A)** Detection of PAXX in spleens and thymi of *Paxx*$^{+/+}$, *Paxx*$^{+/-}$, and *Paxx*$^{-/-}$ mice. Knockout confirmed by the absence of PAXX protein. **B)** Detection of XLF in spleens and thymi of *Xlf*$^{+/+}$, *Xlf*$^{+/-}$, and *Xlf*$^{-/-}$ mice. Knockout confirmed by the absence of XLF protein. **C)** Detection of p53 using Invitrogen Mouse Anti-Human p53 (MA5-12571) to test for cross-reactivity with murine p53. Bands around expected p53 size observed in all samples, including Trp53$^{-/-}$. **D)** Detection of p53 using Santa Cruz Mouse Anti-Human p53 (sc-126) to test for cross-reactivity with murine p53. Bands around expected p53 size were observed in all samples. **E)** Detection of p53 using Santa Cruz Rabbit Anti-Human p53 (sc-6243) to test for cross-reactivity with murine p53. Human HAP1 WT cell lysates (40µg protein) were used as a positive control. No bands around expected p53 size were observed in splenic protein extracts from *Trp53*$^{+/+}$ or *Trp53*$^{-/-}$ mice. Two bands around 45-50kDa (p53*) were observed in HAP1 WT cells. **F)** The same bands observed at 25 and 50kDa in C) and D) were also observed when detecting β-actin in splenic protein extracts from *Trp53*$^{+/+}$ and *Trp53*$^{-/-}$ mice using Mouse Anti-β-actin secondary antibody.

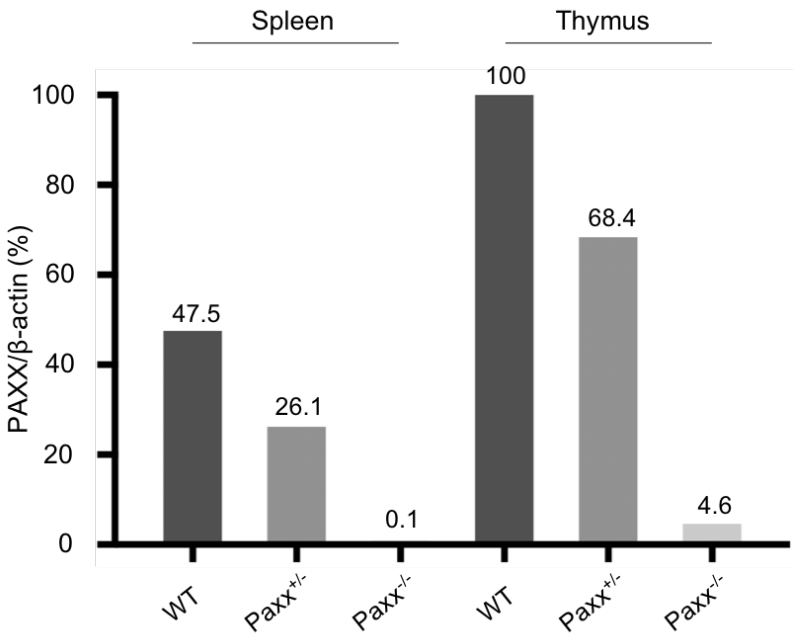

Figure 4.5: Quantification of PAXX protein in spleens and thymi of WT, heterozygous, and knockout mice, normalized by the loading control, β-actin (%). Background levels indicated for the *Paxx*$^{-/-}$ mouse in spleen and thymus. Quantification based on western blot presented in Figure 4.4A. PAXX expression in WT thymus was used as a reference value.

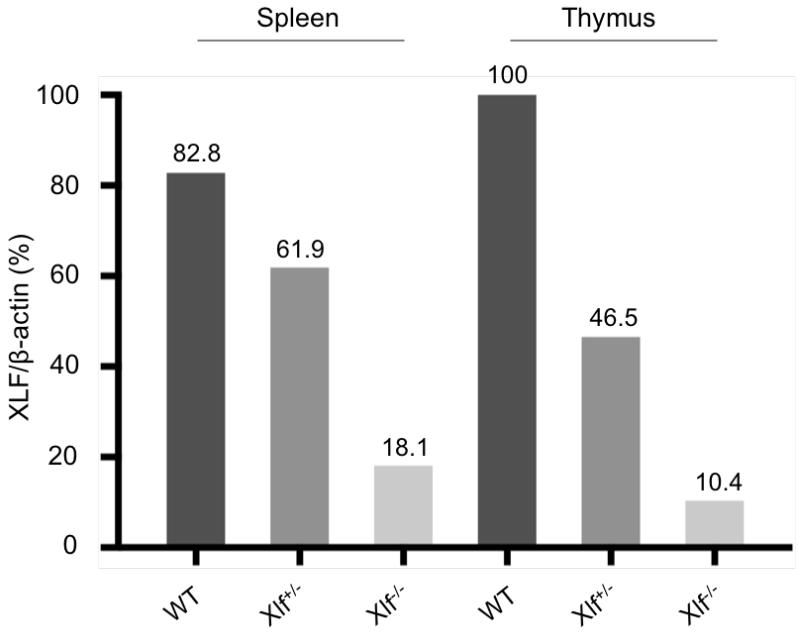

Figure 4.6: Quantification of XLF protein in spleens and thymi of WT, heterozygous, and knockout mice, normalized by the loading control, β-actin (%). Background levels indicated for the Xlf$^{-/-}$ mouse in spleen and thymus. Quantification based on western blot presented in Figure 4.4B. XLF expression in WT thymus was used as a reference value.

4.4 B and T Cell Frequencies in Lymphoid Organs

Splenocytes and thymocytes from "*Paxx*$^{-/-}$" (*n*=3) and control (*n*=3) mice were isolated, stained, and analyzed by flow cytometry to determine whether the B and T cell frequencies were affected by *Paxx* inactivation. Only one pure *Paxx*$^{-/-}$ and one WT mouse was available at the time of experiment. *Trp53*$^{+/-}$ mice were analyzed as PAXX-proficient controls, and *Paxx*$^{-/-}$ *Trp53*$^{+/-}$ mice were analyzed as PAXX-deficient. Splenocytes were stained with Anti-CD19 and Anti-CD3 to determine the proportion of B and T cells, and with Anti-CD4 and Anti-CD8 to determine the proportion of CD4^{+} and CD8^{+} T cells. The thymic proportion of DN, DP, and SP thymocytes was determined by Anti-CD4 and Anti-CD8 double staining. Mice were pooled together for statistics; WT with *Trp53*$^{+/-}$ mice, and *Paxx*$^{-/-}$ with *Paxx*$^{-/-}$*Trp53*$^{+/-}$ mice. All mice except for the pure WT mouse (5.5 weeks) were 7 weeks of age and from the same breeding line. Splenic and thymic cell frequencies are presented in Table 4.1 and 4.2, respectively. Flow cytometric analysis of all mice, comparisons, and *p*-values are presented in Appendix E, p. XI.

Table 4.1: Splenic B and T cell frequencies (%) among controls (WT and *Trp5*$^{+/-}$) and PAXX-deficient (*Paxx*$^{-/-}$ and *Paxx*$^{-/-}$*Trp53*$^{+/-}$) mice analyzed by flow cytometry. CD3^{+}, T cells; CD19^{+}, B cells; CD3^{-}CD19^{-}, other cells residing in the spleen; CD4^{+}, T_H cells; CD8^{+}, T_C cells; CD4^{-}CD8^{-}, B cells and other cells residing in the spleen. RBCs were lysed prior to flow cytometric analysis and are thus not taken into account.

	Cell frequencies, spleen (%)					
	CD3^{+}	**CD19^{+}**	**CD3^{-}CD19^{-}**	**CD4^{+}**	**CD8^{+}**	**CD4^{-}CD8^{-}**
WT	19.3	60.8	18.2	12.7	12.2	73.9
Trp53$^{+/-}$	25.3	52.7	20.2	15.3	12.2	71.7
Trp53$^{+/-}$	22.7	49.6	25.4	13.0	10.1	76.2
Paxx$^{-/-}$	25.2	45.1	27.5	17.3	12.7	69.2
Paxx$^{-/-}$*Trp53*$^{+/-}$	21.4	54.3	22.1	14.2	12.8	71.1
Paxx$^{-/-}$*Trp53*$^{+/-}$	21.9	55.3	20.9	14.7	13.2	71.2

Table 4.2: Thymic DN, DP, and SP T cell frequencies (%) among controls (WT and *Trp5*$^{+/-}$) and PAXX-deficient (*Paxx*$^{-/-}$ and *Paxx*$^{-/-}$*Trp53*$^{+/-}$) mice analyzed by flow cytometry. CD4^{-}CD8^{-}, progenitor T cells; CD4^{+}CD8^{+}, double positive T cells; CD4^{+}, T_H cells; CD8^{+}, T_C cells. RBCs were lysed prior to flow cytometric analysis and are thus not taken into account.

	Cell frequencies, thymus (%)			
	CD4^{-}CD8^{-}	**CD4^{+}CD8^{+}**	**CD4^{+}**	**CD8^{+}**
WT	5.64	82.4	7.62	4.36
Trp53$^{+/-}$	4.16	86.6	6.11	3.12
Trp53$^{+/-}$	4.23	85.0	6.98	3.83
Paxx$^{-/-}$	3.30	89.3	4.89	2.53
Paxx$^{-/-}$*Trp53*$^{+/-}$	4.30	87.5	5.43	2.79
Paxx$^{-/-}$*Trp53*$^{+/-}$	3.31	86.9	6.75	3.00

Examples from flow cytometric analysis of Anti-CD3/Anti-CD19 and Anti-CD4/Anti-CD8 stained splenocytes are presented in Figure 4.7A and 4.8A, respectively. There was no significant difference in splenic B and T cell fractions (Figure 4.7B and C) or splenic CD4^{+} and CD8^{+} fractions (Figure 4.8B and C) among PAXX-deficient mice and controls.

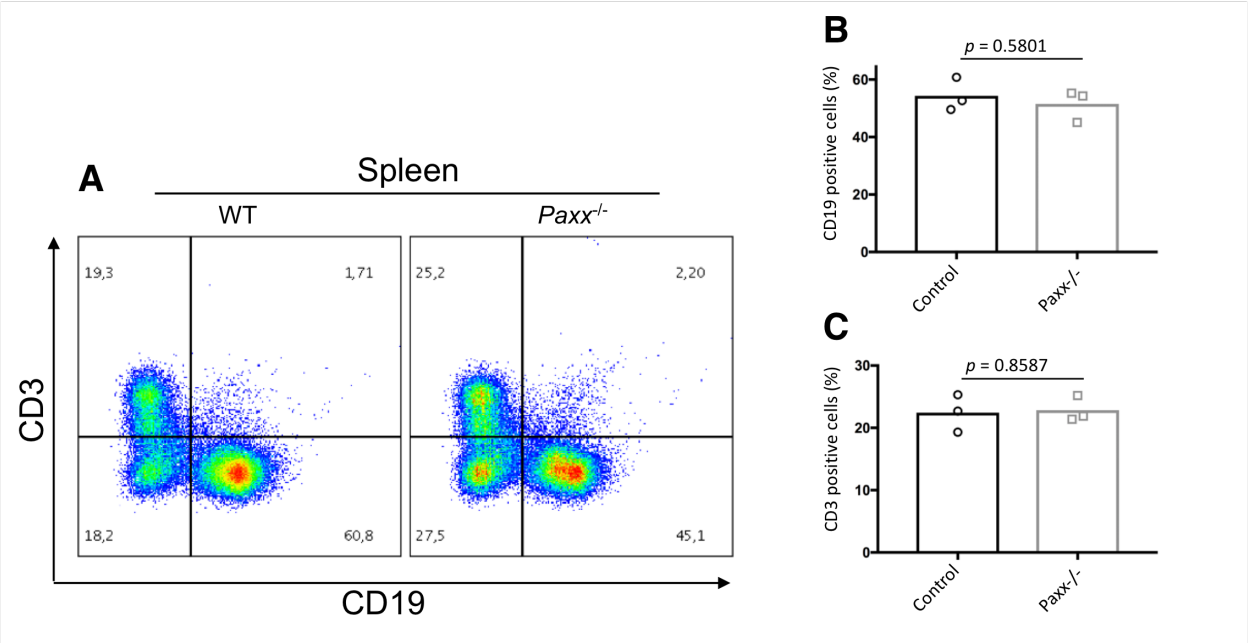

Figure 4.7: Splenic B and T cell frequencies in PAXX-deficient and control mice. **A)** Flow cytometric analysis of splenocytes from WT and *Paxx-/-* mice stained with Anti-CD3 (T cell marker) and Anti-CD19 (B cell marker), frequencies (%) indicated. **B)** Comparison in CD19 positive splenocytes (%) among controls (n=3) and PAXX-deficient (n=3) mice. **C)** Comparison in CD3 positive splenocytes (%) among controls and PAXX-deficient mice. The columns in B) and C) represents the mean. The p-value of each comparison is indicated.

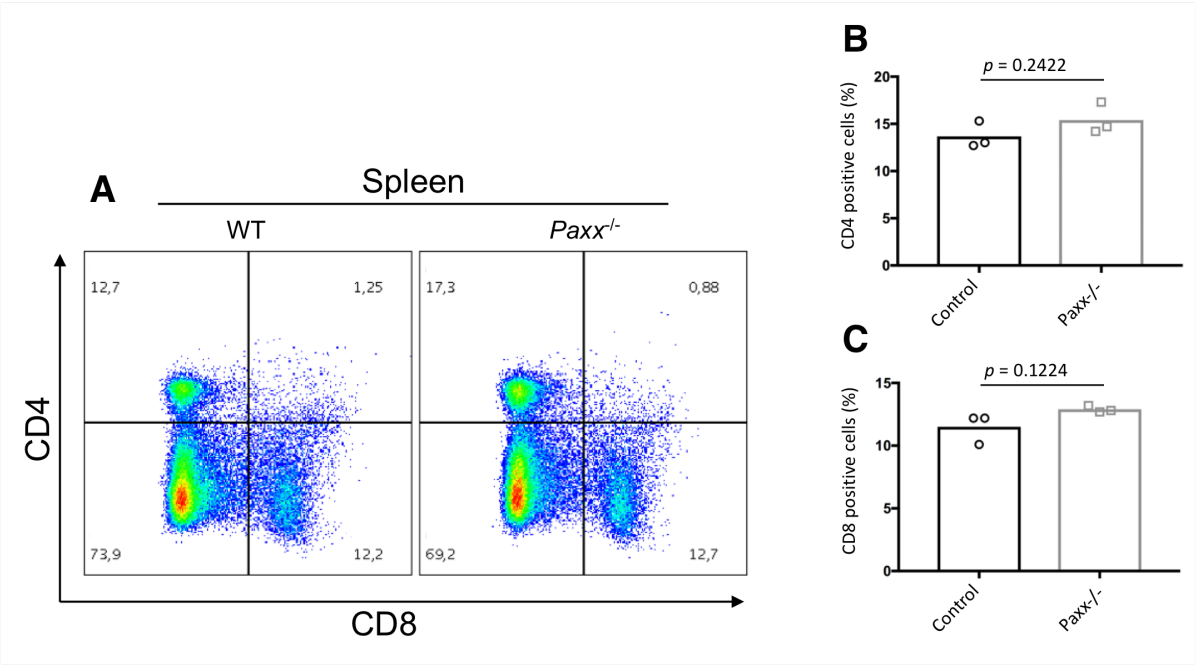

Figure 4.8: Splenic CD4/CD8 T cell frequencies. **A)** Flow cytometric analysis of splenocytes from WT and *Paxx*$^{-/-}$ mice stained with Anti-CD4 and Anti-CD8, frequencies (%) indicated **B)** Comparison in CD4 positive splenocytes (%) among controls (n=3) and PAXX-deficient (n=3) mice. **C)** Comparison in CD8 positive splenocytes (%) among controls and PAXX-deficient mice. The columns in B) and C) represents the mean. The p-value of each comparison is indicated.

An example from flow cytometric analysis of Anti-CD4/Anti-CD8 stained thymocytes is presented in Figure 4.9A. There was no significant difference in double positive ($CD4^+CD8^+$) or single positive ($CD4^+$, $CD8^+$) thymocytes among PAXX-deficient and control mice (Figure 4.9B, C, and D).

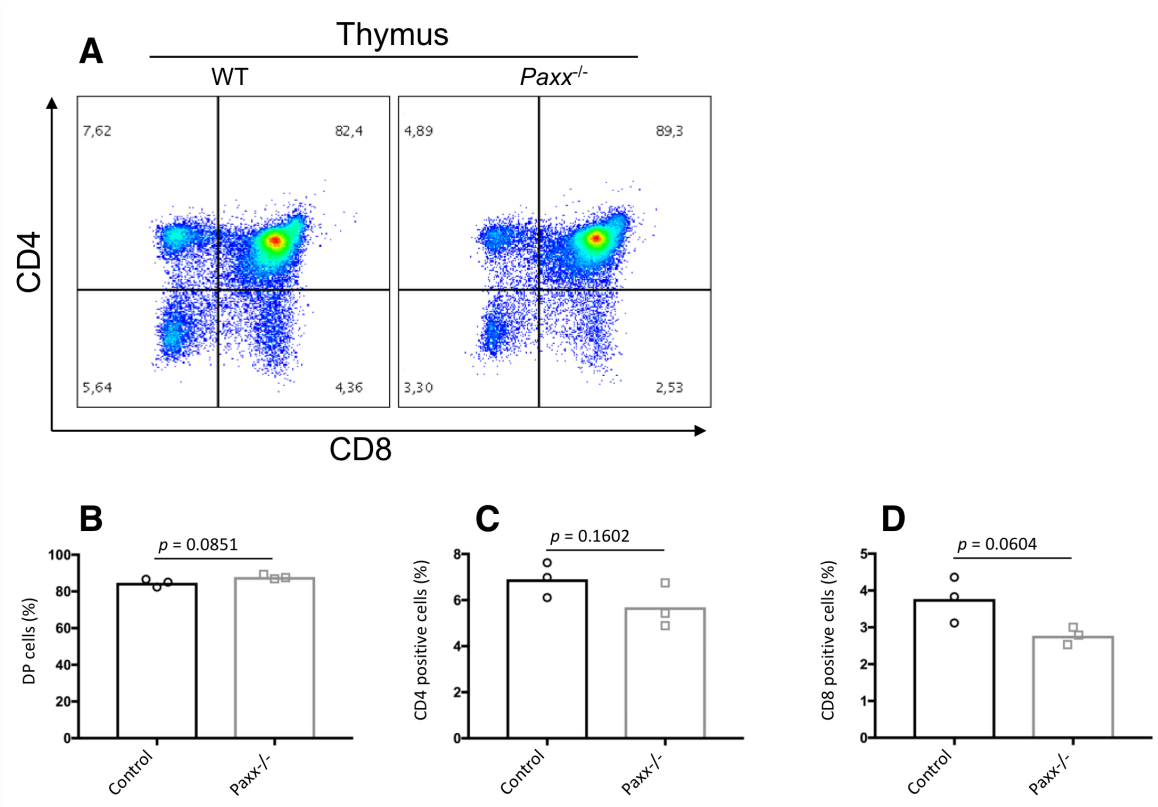

Figure 4.9: Thymic CD4/CD8 T cell frequencies. **A)** Flow cytometric analysis of thymocytes from WT and *Paxx*$^{-/-}$ mice stained with Anti-CD4 and Anti-CD8, frequencies (%) indicated. **B)** Comparison in double positive T cells (%) among controls (n=3) and PAXX-deficient (n=3) mice. **C)** Comparison in CD4 positive thymocytes (%) among controls and PAXX-deficient mice. **D)** Comparison in CD8 positive thymocytes (%) among controls and PAXX-deficient mice. The columns in B), C), and D) represents the mean. The p-value of each comparison is indicated.

4.5 *Paxx.Xlf.Trp53* Breeding

Combined deficiency of PAXX and XLF results in embryonic lethality in mice, complicating the ability to investigate double deficiency *in vivo*. Based on previous findings by our and other research groups[39-41], inactivation of one or both alleles of *Trp53* (encoding p53) has been proposed to rescue the lethality of this double deficiency in mice. Mice heterozygous for *Paxx* and mice heterozygous for *Xlf* were initially crossed. Later, *Paxx*$^{+/-}$*Xlf*$^{+/-}$ mice were crossed with *Trp53*$^{+/-}$ mice to obtain suitable genotypes for further breeding. Later, *Paxx*$^{+/-}$*Xlf*$^{+/-}$*Trp53*$^{+/-}$ mice were crossed with each other, and *Paxx*$^{+/-}$*Xlf*$^{+/-}$*Trp53*$^{+/-}$ crossed with *Paxx*$^{+/-}$*Xlf*$^{+/-}$*Trp53*$^{+/-}$. In total, 64 pups were screened. The distribution of analyzed mice is presented in Table 4.3. Viable *Paxx*$^{-/-}$*Xlf*$^{-/-}$*Trp53*$^{+/+}$ pups were not expected due to embryonic lethality. No *Paxx*$^{-/-}$*Xlf*$^{-/-}$*Trp53*$^{+/-}$ or *Paxx*$^{-/-}$*Xlf*$^{-/-}$*Trp53*$^{-/-}$ mice were identified during this project.

Table 4.3: All possible *Paxx.Xlf.Trp53* genotypes of pups and the number of pups identified for each genotype. In total, 64 pups were screened. Genotypes in bold indicate desired genotypes to investigate double deficiency of PAXX and XLF *in vivo*.

Possible genotypes	**Pups**
Paxx$^{+/+}$*Xlf*$^{+/+}$*Trp53*$^{+/+}$	-
Paxx$^{+/+}$*Xlf*$^{+/+}$*Trp53*$^{+/-}$	5
Paxx$^{+/+}$*Xlf*$^{+/+}$*Trp53*$^{-/-}$	-
Paxx$^{+/+}$*Xlf*$^{+/-}$*Trp53*$^{+/+}$	4
Paxx$^{+/+}$*Xlf*$^{+/-}$*Trp53*$^{+/-}$	-
Paxx$^{+/+}$*Xlf*$^{+/-}$*Trp53*$^{-/-}$	1
Paxx$^{+/+}$*Xlf*$^{-/-}$*Trp53*$^{+/+}$	2
Paxx$^{+/+}$*Xlf*$^{-/-}$*Trp53*$^{+/-}$	7
Paxx$^{+/+}$*Xlf*$^{-/-}$*Trp53*$^{-/-}$	-
Paxx$^{+/-}$*Xlf*$^{+/+}$*Trp53*$^{+/+}$	1
Paxx$^{+/-}$*Xlf*$^{+/+}$*Trp53*$^{+/-}$	2
Paxx$^{+/-}$*Xlf*$^{+/+}$*Trp53*$^{-/-}$	2
Paxx$^{+/-}$*Xlf*$^{+/-}$*Trp53*$^{+/+}$	6
Paxx$^{+/-}$*Xlf*$^{+/-}$*Trp53*$^{+/-}$	9
Paxx$^{+/-}$*Xlf*$^{+/-}$*Trp53*$^{-/-}$	3
Paxx$^{+/-}$*Xlf*$^{-/-}$*Trp53*$^{+/+}$	4
Paxx$^{+/-}$*Xlf*$^{-/-}$*Trp53*$^{+/-}$	7
Paxx$^{+/-}$*Xlf*$^{-/-}$*Trp53*$^{-/-}$	4
Paxx$^{-/-}$*Xlf*$^{+/+}$*Trp53*$^{+/+}$	2
Paxx$^{-/-}$*Xlf*$^{+/+}$*Trp53*$^{+/-}$	3
Paxx$^{-/-}$*Xlf*$^{+/+}$*Trp53*$^{-/-}$	-
Paxx$^{-/-}$*Xlf*$^{+/-}$*Trp53*$^{+/+}$	-
Paxx$^{-/-}$*Xlf*$^{+/-}$*Trp53*$^{+/-}$	1
Paxx$^{-/-}$*Xlf*$^{+/-}$*Trp53*$^{-/-}$	1
Paxx$^{-/-}$*Xlf*$^{-/-}$*Trp53*$^{+/+}$	-
***Paxx*$^{-/-}$*Xlf*$^{-/-}$*Trp53*$^{+/-}$**	-
***Paxx*$^{-/-}$*Xlf*$^{-/-}$*Trp53*$^{-/-}$**	-
Total	64

5 Discussion

5.1 Growth and Immune System Development

In general agreement with previously published *Paxx* knockout mouse models[13, 15, 16, 48], *Paxx*$^{+/-}$ and *Paxx*$^{-/-}$ do not differ from WT mice in growth and immune system development. However, PAXX-deficient mice analyzed during this project showed a reduced number of splenocytes compared to WT mice, an observation also made by Balmus, G., *et al*.[16]. This was also true when grouping genders separately (not shown). PAXX have proven to be non-essential for V(D)J recombination[13, 19], and it has been demonstrated that the ratio of splenic B and T cell populations in PAXX-deficient mice are similar to WT mice[13], suggesting normal development of lymphocytes in the absence of PAXX. The reduction in splenocytes may thus be a result of mild defects in general DNA repair and/or proliferation rather than impairment of V(D)J recombination. Despite reduction in splenocyte cellularity, *Paxx*$^{-/-}$ mice were significantly different from both NHEJ-defective controls in all comparisons made, except from DNA-PKcs-deficient mice in femoral bone marrow cell counts.

The previously described *Xlf* knockout mouse model that was used in this project[18] was analyzed for comparison with our *Paxx* mice. In accordance with Li, G., *et al*.[18] and Vera, G., *et al*. (distinct *Xlf* mouse model)[17], our XLF-deficient mice had a reduction in lymphoid cell counts in both spleen and thymus. In addition, our *Xlf*$^{-/-}$ mice showed a reduction in thymus weight compared to the WT. Vera, G., *et al*.[17] found that the viability of thymocytes was decreased in XLF-deficient mice due to p53-mediated apoptosis, which is a possible explanation for the reduced thymocyte count observed during this project. Similar to PAXX, XLF is not essential for V(D)J recombination due to compensatory mechanisms. Li, G., *et al*.[18] demonstrated that XLF-deficient pro-B cell lines rearrange *V, D,* and *J* segments at nearly WT levels, and Vera, G., *et al*.[17] demonstrated proficient V(D)J recombination in purified DN thymocytes *ex vivo*. The reduced lymphoid cell counts observed might thus be a combination of reduced T cell viability and a mild defect in general DNA repair.

Paxx$^{-/-}$ and *Xlf*$^{-/-}$ knockout mice did not significantly differ from each another in any comparisons made, but the reduction in thymus weight and reduced cellularity of splenocytes and thymocytes was more evident in XLF-deficient mice compared to PAXX-deficient mice. Based on results obtained during this project, *Xlf*$^{-/-}$ mice resemble the NHEJ-defective controls more than what *Paxx*$^{-/-}$ mice do. This supports a more central role of XLF in immune system development, and likely in general DNA repair, than that of PAXX[19].

Both Ku80- and DNA-PKcs-deficient controls had some residual cells in spleens and thymi. These cells correspond to progenitor T cells in the thymus, and other populations of immune cells in the spleen. *Ku80*$^{-/-}$ mice had a significantly lower bone marrow cell count than WT, *Paxx*$^{+/-}$, and *Paxx*$^{-/-}$ mice, whereas the bone marrow cell count in *DNA-PKcs*$^{-/-}$ mice revealed no significant difference when compared to any other genotype. Like *Ku80*$^{-/-}$ mice, DNA-PKcs-deficient mice have a SCID phenotype and were thus predicted to differ from the WT in bone marrow cell counts due to a block in B cell development and mild defects in general DNA repair[49]. There was a certain variation in bone marrow cell counts within groups, including counts among *DNA-PKcs*$^{-/-}$ mice. This may partly be explained by the procedure performed when isolating bone marrow. More accurate isolation procedures may have shifted the result, but a choice of being consistent throughout the project was made. For future experiments, the isolation-procedure should be optimized to ensure reliable results. In addition, the sample size of both *DNA-PKcs*$^{-/-}$ and *Ku80*$^{-/-}$ mice was rather small (n=4 and n=3, respectively). A larger sample size would have reduced random error and thus increased the chance of finding significant differences, given that they exist.

Due to the importance of Ku80 in NHEJ during growth and development, deficiency in mice have shown to reduce the body weight by 40-60% compared to WT mice[50]. Here, *Ku80*$^{-/-}$ mice were significantly smaller than WT and *Paxx*$^{+/-}$ mice, but statistical analysis did not reveal significant differences among *Ku80*$^{-/-}$ and *Paxx*$^{-/-}$, *Xlf*$^{-/-}$, or *DNA-PKcs*$^{-/-}$. This was most likely due to the small sample size[48].

5.2 Protein Expression in Lymphoid Organs

Protein quantification of western blots indicates that there was a 52.5% decrease in splenic PAXX expression compared to thymic PAXX expression in the WT mouse. Reduced expression of PAXX in the spleen compared to thymus have previously been observed[48], and was also observed in a distinct blot with independent mice (Appendix D, p. IX). XLF was expressed at somewhat similar levels in WT organs in contrast to PAXX; the splenic expression of XLF was reduced by 17.5% compared to the expression in thymus. Both PAXX and XLF are widely expressed in all human tissues, but XLF is expressed at higher levels than PAXX in the immune system[55, 56]. Western blots indicate that, at least in the murine spleen, XLF is expressed at higher levels than PAXX. The requirement of PAXX and XLF is also tissue-specific; NHEJ in non-lymphoid cells is compromised by isolated PAXX and XLF deficiencies [5, 10, 11, 18], whereas single PAXX or XLF knockout lymphoid cells are less affected due to compensatory mechanisms during end-ligation (*e.g.* RAG1/2, or ATM and its downstream factors)[12, 21, 57].

Mice heterozygous for *Paxx* and *Xlf* had a reduction in protein expression in both spleen and thymus compared to the WT. Reduction in PAXX expression in liver samples from $Paxx^{+/-}$ mice and in $Paxx^{+/-}$ mouse tail fibroblasts (MTFs) have previously been observed[48]. Reduced PAXX expression in heterozygous mice was also observed in a previous blot with independent mice (Appendix D, p. IX). Having only one functional *Paxx* allele is thus not sufficient for protein expression at WT levels. However, PAXX-haplodeficiency did not cause a detectable phenotype despite reduction of PAXX protein in both spleen (45.1% reduction) and thymus (31.6% reduction); $Paxx^{+/-}$ mice are indistinguishable from WT mice in relation to growth and immune system development. Heterozygous mice are thus PAXX-haplosufficient.

Protein quantification of PAXX and XLF was based on few experimental replicates, and statistics could not be performed to verify whether these observations were reliable or just a result of random biological variation among mice and/or experimental variation. In addition, more accurate quantification methods could have been used. It could have been interesting to further investigate whether XLF is indeed expressed at higher levels than PAXX in murine lymphoid organs, which is the case in humans, and verify that thymic PAXX levels are higher than PAXX levels in the spleen.

In case of viable *Paxx*$^{-/-}$*Xlf*$^{-/-}$*Trp53*$^{-/-}$ or *Paxx*$^{-/-}$*Xlf*$^{-/-}$*Trp53*$^{+/-}$ mice, the protein expression of PAXX, XLF, and p53 was investigated individually. Two Mouse Anti-Human p53 antibodies were initially tested for cross-reactivity with murine p53 (53kDa). The first antibody (Figure 4.4C, Invitrogen, MA5-12571**)** recognize p53 of human origin[G], and the second (Figure 4.4D, Santa Cruz, sc-126) recognize residues 11-25 at the N-terminal of p53 of human origin. Bands around 25, 40, and 50kDa were observed using both antibodies, where the band around 50kDa was of most interest due to the expected size of p53 at about 53kDa. Bands around 50kDa were also present in *Trp53* knockout samples from both spleen and thymus. The genotypes of these mice were verified three times with independent DNA samples, and 50kDa bands were thus thought to be unspecific. For WT and heterozygous mice, there might have been a combination of specific and unspecific bands. No other control in the form of *Trp53*$^{-/-}$ cells (*e.g*. human cell lines) was available at the time to verify this. As both primary antibodies were raised in mice and the target protein was of murine origin, it was not unexpected to observe unspecific bands recognized by the Anti-Mouse secondary antibody. To investigate whether the bands were due to unspecific binding of murine proteins by the Anti-Mouse secondary antibody, a Rabbit Anti-Human p53 antibody (Figure 4.4E, Santa Cruz, sc-6243) having epitopes mapping within full-length p53 of human origin was tested on splenic protein extracts from *Trp53*$^{+/+}$ and *Trp53*$^{-/-}$ mice, along with human HAP1 WT cell lysates as a positive control. Here, previously observed bands around 50kDa were absent in both WT and *Trp53*$^{-/-}$ samples, suggesting that previously observed bands were unspecific. Two bands in the detection range of p53 were observed for HAP1 cells (around 45-50kDa). These might be different isoforms of p53, modified p53, or a combination of specific and unspecific bands. No negative control was available to verify this at the time. When detecting β-actin for the same blot using Mouse Anti-β-actin (Figure 4.4F), the same bands previously observed appeared in the samples from *Trp53*$^{+/+}$ and *Trp53*$^{+/-}$ mice. It is possible that these bands correspond to heavy (~50kDa) and light (~25kDa) chains of murine IgG present in the protein extracts, that was recognized by the secondary antibody (Anti-Mouse). This would explain why these bands were also present in the *Trp53* knockout. To avoid potential interference between IgG H-chains (50kDa) and p53 (53kDa), primary antibodies raised in a different species rather than the one being investigated, or antibodies only recognizing the L-chain could have been tested.

[G] Epitope not stated in the antibody datasheet

Further optimization of each antibody is needed before concluding whether they work or not. As already noted, the similarity in size of p53 and the unspecific bands observed using Mouse Anti-Human primary antibodies complicates the interpretation of the western blots in absence of a proper negative control; there might be several bands in close approximation to each other in *Trp53*$^{+/+}$ and *Trp53*$^{+/-}$ samples. No band around expected p53 size was observed in the splenic WT sample when using the Rabbit Anti-Human (sc-6243) antibody. It might be that the splenic expression was too low to be detected, as the p53 protein is known to be expressed at low levels in normal cells[58]. To test if this was due to protein levels too low to be detected, cells could have been treated with DNA damaging agents (*e.g.* IR, UV, H_2O_2, or etoposide) prior to lysis to induce cellular stress, and thus upregulation of p53. Another potential explanation is that the antibodies are incapable of sufficient recognition of murine p53. Murine p53 protein sequences (two isoforms) differ from human sequences (12 isoforms) in both length and in several amino acid residues. A protein BLAST revealed that both *a* and *b* murine p53 isoforms resemble human p53 isoform *a* the most, with a 77% identity and 82% similarity (Appendix F, p. XV). These differences in protein sequence might be enough for insufficient recognition by the Anti-Human p53 antibodies.

5.3 B and T Cell Frequencies in Lymphoid Organs

Two *Trp53*$^{+/-}$ and two Paxx$^{-/-}$*Trp53*$^{+/-}$ mice were analyzed along with WT and *Paxx*$^{-/-}$ mice to compare B and T cell fractions among the two groups; PAXX-proficient and PAXX-deficient. Jiang, W., *et al*.[7] and Frank, K.M., *et al*.[41] have demonstrated that the inactivation of one *Trp53* allele does not affect the development of lymphocytes and that heterozygous *Trp53* mice resemble WT mice. For statistics, groups of pure WTs and *Paxx*$^{-/-}$ mice would have been ideal, but the availability of mice was limited at the time of experiments. Flow cytometric analysis of all mice, comparisons, and *p*-values are presented in Appendix E, p. XI.

There was no difference in splenic B and T cell fractions among PAXX-deficient mice and controls, and the observed fractions in both groups were consistent with expected murine lymphocyte frequencies. The spleen is a secondary lymphoid organ where only mature B and T cells, other immune cells, and RBCs reside. The observed reduction in splenocyte counts in *Paxx*$^{-/-}$ mice are thus not thought to be a result of impaired V(D)J recombination, based on the normal fraction of splenic B and T cells. After RBC lysis, the double negative (CD3^{-}CD19^{-}) population of splenocytes corresponds to other cells of the immune system such as monocytes, granulocytes, natural killer cells, and dendritic cells. CD19 is not expressed on terminally differentiated plasma cells (mature B cell linage), and these B cells would thus be part of the double negative population.

There was no difference in splenic CD4^{+} or CD8^{+} cells, or CD4^{-}CD8^{-} cells among PAXX-deficient mice and controls. The double negative population correspond to B cells and other immune cells residing in the spleen. Fractions of CD4^{+} and CD8^{+} cells are consistent with expected frequencies in murine spleens.

The fractions of double negative (CD4^{-}CD8^{-}), double positive (CD4^{+}CD8^{+}), and single positive (CD4^{+}, CD8^{+}) thymocytes were not significantly different among PAXX-deficient mice and control mice. The double negative population corresponds to developing T cells (DN1-DN4).

Originally, the goal was to investigate the frequencies of pro- ($CD43^+B220^+IgM^-$), pre- ($CD43^-B220^+IgM^-$), and immature ($CD43^-B220^+IgM^+$) B cell populations in bone marrow isolated from *Paxx*$^{-/-}$ and control mice, to determine any possible differences among the two groups. This was not achieved due to time limitation, and staining-protocols/antibodies in need of optimization. However, based on observed splenic B cell fractions ($CD19^+$ splenocytes) in PAXX-deficient mice, the development of B cells appears to be normal. The normal B cell frequency indicates that the B cell development in bone marrow is likely not impaired in the absence of PAXX, which is in accordance with Liu, X., *et al*.[13]. However, optimization of staining-protocols and antibodies (CD43, B220, and IgM) would have been ideal for determining whether B cell development is affected by *Paxx* inactivation, by comparing the pro-, pre-, and immature B cell populations in PAXX-deficient and control mice.

5.4 *Paxx.Xlf.Trp53* Breeding

Sixty-four *Paxx.Xlf.Trp53* mice were analyzed during this project, but no *Paxx*$^{-/-}$*Xlf*$^{-/-}$*Trp53*$^{+/-}$ or *Paxx*$^{-/-}$*Xlf*$^{-/-}$*Trp53*$^{-/-}$ mice were identified. The genes encoding PAXX, XLF and p53 in mice are all located on different chromosomes (murine chromosome 2, 1, and 11, respectively). Based on independent assortment of alleles it should be possible to get triple knockouts and *Paxx*$^{-/-}$*Xlf*$^{-/-}$*Trp53*$^{+/-}$ mice, given that these mice are viable. The probability of getting either one of these genotypes when crossing triple heterozygous mice is 3/64, and 3/32 when crossing triple heterozygous mice with *Paxx*$^{+/-}$*Xlf*$^{-/-}$*Trp53*$^{+/-}$ mice. More mice need to be analyzed before any conclusion about viability can be made.

Crossing XRCC4- and Lig4-deficient mice into a p53 background have shown to rescue neuronal apoptosis and embryonic lethality, but the mice were smaller, retained their SCID phenotype, and were prone to B cell lymphomas due to unresolved RAG-induced DSBs and translocations[40, 41, 59]**.** Due to the phenotypic similarities shared among *Xrcc4*$^{-/-}$, *Lig4*$^{-/-}$, and *Paxx*$^{-/-}$*Xlf*$^{-/-}$ mice, this could possibly be the case in *Paxx*$^{-/-}$*Xlf*$^{-/-}$*Trp53*$^{+/-}$ and *Paxx*$^{-/-}$*Xlf*$^{-/-}$*Trp53*$^{-/-}$ mice as well. If these mice prove to be viable, it would allow *in vivo* studies of double knockout *Paxx* and *Xlf* mice. Further investigation of overlapping and non-overlapping functions among these two proteins would enhance the current understanding of PAXX and XLF function, and thus NHEJ in general.

6 Conclusion

Western blot analysis and protein quantification indicate that inactivation of one *Paxx* allele results in mice unable to express PAXX at WT levels in spleen and thymus. PAXX also appears to be expressed at higher levels in the thymus compared to the spleen in both WT and heterozygous mice. However, neither reduced expression of PAXX nor absence of PAXX affect growth or immune system development in $Paxx^{+/-}$ or $Paxx^{-/-}$ mice; these mice are indistinguishable from WT mice. Flow cytometric analysis of splenocytes and thymocytes isolated from PAXX-deficient mice revealed normal B and T cell frequencies that were not significantly different from PAXX-proficient frequencies, indicating normal development of lymphocytes in the absence of PAXX. Only B and T lymphocytes with successfully rearranged antigen receptors are expected in the spleen, indicating that the reduced splenocyte count observed in PAXX-deficient mice might be a consequence of mild defects in general DNA repair and/or impairment of proliferation, rather than a defect in V(D)J recombination during lymphocyte development. Based on these findings, it is here concluded that PAXX-deficient mice are comparable to WT mice, conferring no overt phenotype in relation to growth and immune system development.

PAXX- and XLF-deficient mice did not significantly differ from each other in any comparisons made, but the reduction in thymus weight and reduced cellularity of splenocytes and thymocytes was more evident in the latter. The reduced cellularity in $Xlf^{-/-}$ mice might be a result of impaired T cell viability, proliferation, and/or mild defects in general DNA repair. In addition, XLF-deficient mice resembled NHEJ-defective controls to a greater extent than what PAXX-deficient mice did. Together, these findings indicate a more central role of XLF in NHEJ than that of PAXX.

Among the 64 *Paxx.Xlf.Trp53* pups analyzed, no $Paxx^{-/-}Xlf^{-/-}Trp53^{+/-}$ or $Paxx^{-/-}Xlf^{-/-}Trp53^{-/-}$ mice were identified. More mice need to be analyzed before any conclusion about viability of these complex mutants can be made. If these mice prove to be viable, this would allow *in vivo* studies of double-deficient PAXX and XLF mice. Further investigation of overlapping and non-overlapping functions between PAXX and XLF would enhance the current understanding of the functional interaction between these two proteins, and thus the NHEJ pathway in general.

7 References

1. Iyama, T. and D.M. Wilson, 3rd, *DNA repair mechanisms in dividing and non-dividing cells.* DNA Repair (Amst), 2013. **12**(8): p. 620-36.
2. Rulten, S.L. and G.J. Grundy, *Non-homologous end joining: Common interaction sites and exchange of multiple factors in the DNA repair process.* Bioessays, 2017. **39**(3).
3. Hentges, P., et al., *Evolutionary and functional conservation of the DNA non-homologous end-joining protein, XLF/Cernunnos.* J Biol Chem, 2006. **281**(49): p. 37517-26.
4. Chang, H.H. and M.R. Lieber, *Structure-Specific nuclease activities of Artemis and the Artemis: DNA-PKcs complex.* Nucleic Acids Res, 2016. **44**(11): p. 4991-7.
5. Ochi, T., et al., *DNA repair. PAXX, a paralog of XRCC4 and XLF, interacts with Ku to promote DNA double-strand break repair.* Science, 2015. **347**(6218): p. 185-188.
6. Chang, H.H.Y., et al., *Non-homologous DNA end joining and alternative pathways to double-strand break repair.* Nat Rev Mol Cell Biol, 2017. **18**(8): p. 495-506.
7. Jiang, W., et al., *Differential phosphorylation of DNA-PKcs regulates the interplay between end-processing and end-ligation during nonhomologous end-joining.* Mol Cell, 2015. **58**(1): p. 172-85.
8. Callebaut, I., et al., *Cernunnos interacts with the XRCC4 x DNA-ligase IV complex and is homologous to the yeast nonhomologous end-joining factor Nej1.* J Biol Chem, 2006. **281**(20): p. 13857-60.
9. Buck, D., et al., *Cernunnos, a novel nonhomologous end-joining factor, is mutated in human immunodeficiency with microcephaly.* Cell, 2006. **124**(2): p. 287-99.
10. Xing, M., et al., *Interactome analysis identifies a new paralogue of XRCC4 in non-homologous end joining DNA repair pathway.* Nat Commun, 2015. **6**: p. 6233.
11. Craxton, A., et al., *XLS (c9orf142) is a new component of mammalian DNA double-stranded break repair.* Cell Death Differ, 2015. **22**(6): p. 890-7.
12. Kumar, V., F.W. Alt, and V. Oksenych, *Functional overlaps between XLF and the ATM-dependent DNA double strand break response.* DNA Repair (Amst), 2014. **16**: p. 11-22.
13. Liu, X., et al., *PAXX promotes KU accumulation at DNA breaks and is essential for end-joining in XLF-deficient mice.* Nat Commun, 2017. **8**: p. 13816.
14. Ahnesorg, P., P. Smith, and S.P. Jackson, *XLF interacts with the XRCC4-DNA ligase IV complex to promote DNA nonhomologous end-joining.* Cell, 2006. **124**(2): p. 301-13.
15. Abramowski, V., et al., *PAXX and Xlf interplay revealed by impaired CNS development and immunodeficiency of double KO mice.* Cell Death Differ, 2018. **25**(2): p. 444-452.
16. Balmus, G., et al., *Synthetic lethality between PAXX and XLF in mammalian development.* Genes & development, 2016. **30**(19): p. 2152.
17. Vera, G., et al., *Cernunnos deficiency reduces thymocyte life span and alters the T cell repertoire in mice and humans.* Mol Cell Biol, 2013. **33**(4): p. 701-11.
18. Li, G., et al., *Lymphocyte-specific compensation for XLF/cernunnos end-joining functions in V(D)J recombination.* Mol Cell, 2008. **31**(5): p. 631-40.
19. Lescale, C., et al., *Specific Roles of XRCC4 Paralogs PAXX and XLF during V(D)J Recombination.* Cell Rep, 2016. **16**(11): p. 2967-2979.
20. Kumar, V., F.W. Alt, and R.L. Frock, *PAXX and XLF DNA repair factors are functionally redundant in joining DNA breaks in a G1-arrested progenitor B-cell line.* Proc Natl Acad Sci U S A, 2016. **113**(38): p. 10619-24.
21. Lescale, C., et al., *RAG2 and XLF/Cernunnos interplay reveals a novel role for the RAG complex in DNA repair.* Nat Commun, 2016. **7**: p. 10529.
22. Woodbine, L., A.R. Gennery, and P.A. Jeggo, *The clinical impact of deficiency in DNA non-homologous end-joining.* DNA Repair (Amst), 2014. **16**: p. 84-96.
23. Owen, J., J. Punt, and S. Standford, *Kuby Immunology*. 2013: Freeman, W. H. & Company. 832.
24. Arya, R. and C.H. Bassing, *V(D)J Recombination Exploits DNA Damage Responses to Promote Immunity.* Trends Genet, 2017. **33**(7): p. 479-489.

25. Pieper, K., B. Grimbacher, and H. Eibel, *B-cell biology and development.* J Allergy Clin Immunol, 2013. **131**(4): p. 959-71.
26. Sandel, P.C. and J.G. Monroe, *Negative selection of immature B cells by receptor editing or deletion is determined by site of antigen encounter.* Immunity, 1999. **10**(3): p. 289-99.
27. BD Biosciences. *Human and Mouse CD Marker Handbook*. Available from: https://www.bdbiosciences.com/documents/cd_marker_handbook.pdf. Accessed: 4th of June, 2018
28. Wang, K., G. Wei, and D. Liu, *CD19: a biomarker for B cell development, lymphoma diagnosis and therapy.* Exp Hematol Oncol, 2012. **1**(1): p. 36.
29. Janeway CA Jr, T.P., Walport M, et al, *The Immune System in Health and Disease*, in *T cell receptor gene rearrangement*. 2001, Garland Science: New York.
30. Birnbaum, M.E., et al., *Molecular architecture of the alphabeta T cell receptor-CD3 complex.* Proc Natl Acad Sci U S A, 2014. **111**(49): p. 17576-81.
31. Hey, Y.Y. and H.C. O'Neill, *Murine spleen contains a diversity of myeloid and dendritic cells distinct in antigen presenting function.* J Cell Mol Med, 2012. **16**(11): p. 2611-9.
32. Bio-Rad. *Flow cytometry - cell frequency*. 2017; Available from: https://www.bio-rad-antibodies.com/flow-cytometry-cell-frequency.html#%E2%80%8BMurine%20cell%20frequency%C2%A0. Accessed: 15th of May, 2018
33. Schatz, D.G. and Y. Ji, *Recombination centres and the orchestration of V(D)J recombination.* Nat Rev Immunol, 2011. **11**(4): p. 251-63.
34. Meek, K., et al., *The ATM Kinase Restrains Joining of Both VDJ Signal and Coding Ends.* J Immunol, 2016. **197**(8): p. 3165-3174.
35. Reinhardt, H.C. and B. Schumacher, *The p53 network: cellular and systemic DNA damage responses in aging and cancer.* Trends Genet, 2012. **28**(3): p. 128-36.
36. Hu, J., et al., *Developmental propagation of V(D)J recombination-associated DNA breaks and translocations in mature B cells via dicentric chromosomes.* Proc Natl Acad Sci U S A, 2014. **111**(28): p. 10269-74.
37. Oksenych, V., et al., *Functional redundancy between the XLF and DNA-PKcs DNA repair factors in V(D)J recombination and nonhomologous DNA end joining.* Proc Natl Acad Sci U S A, 2013. **110**(6): p. 2234-9.
38. Gao, Y., et al., *A critical role for DNA end-joining proteins in both lymphogenesis and neurogenesis.* Cell, 1998. **95**(7): p. 891-902.
39. Xing, M., et al., *Synthetic lethality between murine DNA repair factors XLF and DNA-PKcs is rescued by inactivation of Ku70.* DNA Repair (Amst), 2017. **57**: p. 133-138.
40. Gao, Y., et al., *Interplay of p53 and DNA-repair protein XRCC4 in tumorigenesis, genomic stability and development.* Nature, 2000. **404**(6780): p. 897-900.
41. Frank, K.M., et al., *DNA ligase IV deficiency in mice leads to defective neurogenesis and embryonic lethality via the p53 pathway.* Mol Cell, 2000. **5**(6): p. 993-1002.
42. Riballo, E., et al., *Cellular and biochemical impact of a mutation in DNA ligase IV conferring clinical radiosensitivity.* J Biol Chem, 2001. **276**(33): p. 31124-32.
43. O'Driscoll, M., et al., *DNA ligase IV mutations identified in patients exhibiting developmental delay and immunodeficiency.* Mol Cell, 2001. **8**(6): p. 1175-85.
44. Moshous, D., et al., *Artemis, a novel DNA double-strand break repair/V(D)J recombination protein, is mutated in human severe combined immune deficiency.* Cell, 2001. **105**(2): p. 177-86.
45. van der Burg, M., et al., *A DNA-PKcs mutation in a radiosensitive T-B- SCID patient inhibits Artemis activation and nonhomologous end-joining.* J Clin Invest, 2009. **119**(1): p. 91-8.
46. Woodbine, L., et al., *PRKDC mutations in a SCID patient with profound neurological abnormalities.* J Clin Invest, 2013. **123**(7): p. 2969-80.
47. Saito, S., A. Kurosawa, and N. Adachi, *Mutations in XRCC4 cause primordial dwarfism without causing immunodeficiency.* J Hum Genet, 2016. **61**(8): p. 679-85.
48. Gago-Fuentes, R., et al., *Normal development of mice lacking PAXX, the paralogue of XRCC4 and XLF.* FEBS Open Bio, 2018. **8**(3): p. 426-434.

49. Gao, Y., et al., *A targeted DNA-PKcs-null mutation reveals DNA-PK-independent functions for KU in V(D)J recombination.* Immunity, 1998. **9**(3): p. 367-76.
50. Nussenzweig, A., et al., *Requirement for Ku80 in growth and immunoglobulin V(D)J recombination.* Nature, 1996. **382**(6591): p. 551-5.
51. Jacks, T., et al., *Tumor spectrum analysis in p53-mutant mice.* Curr Biol, 1994. **4**(1): p. 1-7.
52. Bosma, G.C., R.P. Custer, and M.J. Bosma, *A severe combined immunodeficiency mutation in the mouse.* Nature, 1983. **301**(5900): p. 527-30.
53. Blunt, T., et al., *Identification of a nonsense mutation in the carboxyl-terminal region of DNA-dependent protein kinase catalytic subunit in the scid mouse.* Proc Natl Acad Sci U S A, 1996. **93**(19): p. 10285-90.
54. Nussenzweig, A., et al., *Hypersensitivity of Ku80-deficient cell lines and mice to DNA damage: the effects of ionizing radiation on growth, survival, and development.* Proc Natl Acad Sci U S A, 1997. **94**(25): p. 13588-93.
55. The Human Protein Atlas. *NHEJ1*. Available from: https://www.proteinatlas.org/ENSG00000187736-NHEJ1/tissue. Accessed: 5th of June, 2018
56. The Human Protein Atlas. *C9orf142*. Available from: https://www.proteinatlas.org/ENSG00000148362-C9orf142/tissue. Accessed: 5th of June, 2018
57. Hung, P.J., et al., *Deficiency of XLF and PAXX prevents DNA double-strand break repair by non-homologous end joining in lymphocytes.* Cell Cycle, 2017. **16**(3): p. 286-295.
58. Kastenhuber, E.R. and S.W. Lowe, *Putting p53 in Context.* Cell, 2017. **170**(6): p. 1062-1078.
59. Ferguson, D.O. and F.W. Alt, *DNA double strand break repair and chromosomal translocation: lessons from animal models.* Oncogene, 2001. **20**(40): p. 5572-9.

Appendix A: Primers and Expected Amplicons

Table A.1: Primer sequences and expected WT and mutant amplicons of *DNA-PKcs*, *Paxx*, *Scid*, *Trp53*, *Xlf*, and *Ku80*.

Primers	Sequence	Amplicons
DNA-PKcs WT	GAAAAAGTCTATGAGCTCCTGGGAG	WT 250bp / Mutant 427bp
DNA-PKcs Mutant	ACGTAACTCCTCTTCAGACCT	
DNA-PKcs Common	CCCTCCAGACAGCCAGCTAAGACAGG	
Paxx Forward	ACAGAGGGTGGTGACTCAGACAATGG	WT 965bp / Mutant 329, 312, or 295bp
Paxx Reverse	GGAAATGCTATTAGAACCACTGCCACG	
Scid WT	ACAGGCTGTCCTGGAACTC	WT 409bp / Mutant 316bp
Scid Mutant	CCGGTACTTTCCAGCCTCTC	
Scid Common	CACGGTGGAAGACAAGAACA	
Trp53 WT	AGGCTTAGAGGTGCAAGCTG	WT 321bp / Mutant 150bp
Trp53 Mutant	CAGCCTCTGTTCCACATACACT	
Trp53 Common	TGGATGGTGGTATACTCAGAGC	
Xlf WT	CATGTTGGCTCTGCGAATAGA	WT 650bp / Mutant 950bp
Xlf Mutant	CTGTCTTGTGGGCATAGTAGGC	
Xlf Common	GAGCTCGGATATGAGCGCTCAG	
Ku80 WT	AGCTTCCACCCTCTAGAGAT	WT 400bp / Mutant 320bp
Ku80 Mutant	TAAAGCGCATGCTCCAGACT	
Ku80 Common	ATTGTGATGTGTGGGACACG	

Appendix B: PCR Programs

A *DNA PKcs* (WT)

Step	Time	Temperature (°C)	Cycles
Initial denaturation	3 m	94	1
Denaturation	45 s	94	30
Annealing	45 s	66	
Elongation	1 m	72	
Final extension	5 m	72	1
Hold	∞	4	

B *DNA PKcs* (Mut)

Step	Time	Temperature (°C)	Cycles
Initial denaturation	3 m	94	1
Denaturation	45 s	94	40
Annealing	45 s	59	
Elongation	1 m	72	
Final extension	5 m	72	1
Hold	∞	4	

C *Ku80* (WT/Mut)

Step	Time	Temperature (°C)	Cycles
Initial denaturation	2 m	94	1
Denaturation	20 s	94	40
Annealing	15 s	61	
Elongation	40 s	72	
Final extension	5 m	72	1
Hold	∞	4	

D *Paxx* (WT/Mut)

Step	Time	Temperature (°C)	Cycles
Initial denaturation	2 m	94	1
Denaturation	30 s	94	30
Annealing	45 s	68	
Elongation	1 m	72	
Final extension	5 m	72	1
Hold	∞	4	

E *Scid* (WT)

Step	Time	Temperature (°C)	Cycles
Initial denaturation	2 m	95	1
Denaturation	20 s	95	35
Annealing	40 s	54	
Elongation	1 m	72	
Final extension	5 m	72	1
Hold	∞	4	

F *Scid* (Mut)

Step	Time	Temperature (°C)	Cycles
Initial denaturation	2 m	94	1
Denaturation	20 s	94	40
Annealing	15 s	65	
Elongation	35 s	72	
Final extension	5 m	72	1
Hold	∞	4	

G *Trp53* (WT/Mut)

Step	Time	Temperature (°C)	Cycles
Initial denaturation	2 m	95	1
Denaturation	30 s	95	30
Annealing	30 s	67	
Elongation	20 s	72	
Final extension	5 m	72	1
Hold	2 m	95	

H *Xlf* (WT/Mut)

Step	Time	Temperature (°C)	Cycles
Initial denaturation	3 m	95	1
Denaturation	30 s	95	40
Annealing, extention	1 m	62	
Final extension	5 m	68	1
Hold	∞	4	

Figure B.1: All PCR programs used. **A)** DNA-PKcs WT allele. **B)** *DNA-PKcs* mutant allele. **C)** Combined program for *Ku80* WT and mutant alleles. **D)** Combined program for *Paxx* WT and mutant alleles. **E)** *Scid* WT allele. **F)** *Scid* mutant allele. **G)** Combined program for *Trp53* WT and mutant alleles. G) **H)** Combined program for *Xlf* WT and mutant alleles.

Appendix C: Growth and Immune System Development – Averages and Comparisons

Table C.1: Average values in spleen weight, splenocyte count, thymus weight, thymocyte count, bone marrow (BM) cell count, and body weight (BW) in WT, *Paxx*$^{+/-}$, *Paxx*$^{-/-}$, *Xlf*$^{-/-}$, *DNA-PKcs*$^{-/-}$, and *Ku80*$^{-/-}$ mice.

	Spleen (mg)	Splenocytes (millions)	Thymus (mg)	Thymocytes (millions)	BM cells (millions)	BW (g)
WT	70.2	125.1	87.7	281.5	32.7	19.5
Paxx$^{+/-}$	71.5	104.8	79.7	235.6	33.1	17.8
Paxx$^{-/-}$	62.5	77.1	83.1	214.5	26.3	16.6
Xlf$^{-/-}$	53.0	56.5	66.2	130.6	22.4	18.0
DNA-PKcs$^{-/-}$	19.8	10.1	12.5	1.4	19.8	18.2
Ku80$^{-/-}$	13.0	4.2	6.2	0.1	9.0	11.5

Table C.2: Statistical analyzes of spleen weight among WT, *Paxx*$^{+/-}$, *Paxx*$^{-/-}$, *Xlf*$^{-/-}$, *Ku80*$^{-/-}$, and *DNA-PKcs*$^{-/-}$ mice with indicated significance and *p*-values (one-way ANOVA).

Spleen weight	Significance[1]	*p*-value
WT vs. *Paxx*$^{+/-}$	ns	>0.9999
WT vs. *Paxx*$^{-/-}$	ns	0.9002
WT vs. *Xlf*$^{-/-}$	ns	0.4234
WT vs. *Ku80*$^{-/-}$	****	<0.0001
WT vs. *DNA-PKcs*$^{-/-}$	***	0.0001
Paxx$^{+/-}$ vs. *Paxx*$^{-/-}$	ns	0.7274
Paxx$^{+/-}$ vs. *Xlf*$^{-/-}$	ns	0.2523
Paxx$^{+/-}$ vs. *Ku80*$^{-/-}$	****	<0.0001
Paxx$^{+/-}$ vs. *DNA-PKcs*$^{-/-}$	****	<0.0001
Paxx$^{-/-}$ vs. *Xlf*$^{-/-}$	ns	0.8789
Paxx$^{-/-}$ vs. *Ku80*$^{-/-}$	***	0.0004
Paxx$^{-/-}$ vs. *DNA-PKcs*$^{-/-}$	***	0.0006
Xlf$^{-/-}$ vs. *Ku80*$^{-/-}$	*	0.0171
Xlf$^{-/-}$ vs. *DNA-PKcs*$^{-/-}$	*	0.0395
Ku80$^{-/-}$ vs *DNA-PKcs*$^{-/-}$	ns	0.9932

[1] not significant (ns) = $p > 0.05$, * = $p \leq 0.05$, *** = $p \leq 0.001$, **** = $p < 0.0001$

Table C.3: Statistical analyzes of splenocyte cell count among WT, *Paxx*$^{+/-}$, *Paxx*$^{-/-}$, *Xlf*$^{-/-}$, *Ku80*$^{-/-}$, and *DNA-PKcs*$^{-/-}$ mice with indicated significance and *p*-values (one-way ANOVA).

Splenocyte count	Significance[1]	*p*-value
WT vs. *Paxx*$^{+/-}$	ns	0.5115
WT vs. *Paxx*$^{-/-}$	**	0.0041
WT vs. *Xlf*$^{-/-}$	***	0.0003
WT vs. *Ku80*$^{-/-}$	****	<0.0001
WT vs. *DNA-PKcs*$^{-/-}$	****	<0.0001
Paxx$^{+/-}$ vs. *Paxx*$^{-/-}$	ns	0.0851
Paxx$^{+/-}$ vs. *Xlf*$^{-/-}$	**	0.0053
Paxx$^{+/-}$ vs. *Ku80*$^{-/-}$	****	<0.0001
Paxx$^{+/-}$ vs. *DNA-PKcs*$^{-/-}$	****	<0.0001
Paxx$^{-/-}$ vs. *Xlf*$^{-/-}$	ns	0.5942
Paxx$^{-/-}$ vs. *Ku80*$^{-/-}$	***	0.0005
Paxx$^{-/-}$ vs. *DNA-PKcs*$^{-/-}$	***	0.0003
Xlf$^{-/-}$ vs. *Ku80*$^{-/-}$	*	0.0438
Xlf$^{-/-}$ vs. *DNA-PKcs*$^{-/-}$	ns	0.0560
Ku80$^{-/-}$ vs *DNA-PKcs*$^{-/-}$	ns	0.9994

[1] not significant (ns) = $p > 0.05$, * = $p \leq 0.05$, ** = $p \leq 0.01$, *** = $p \leq 0.001$, **** = $p < 0.0001$

Table C.4: Statistical analyzes of thymus weight among WT, *Paxx*$^{+/-}$, *Paxx*$^{-/-}$, *Xlf*$^{-/-}$, *Ku80*$^{-/-}$, and *DNA-PKcs*$^{-/-}$ mice with indicated significance and *p*-values (one-way ANOVA).

Thymus weight	**Significance**[1]	***p*-value**
WT vs. *Paxx*$^{+/-}$	ns	0.5250
WT vs. *Paxx*$^{-/-}$	ns	0.9298
WT vs. *Xlf*$^{-/-}$	*	0.0106
WT vs. *Ku80*$^{-/-}$	****	<0.0001
WT vs. *DNA-PKcs*$^{-/-}$	****	<0.0001
Paxx$^{+/-}$ vs. *Paxx*$^{-/-}$	ns	0.9663
Paxx$^{+/-}$ vs. *Xlf*$^{-/-}$	ns	0.1568
Paxx$^{+/-}$ vs. *Ku80*$^{-/-}$	****	<0.0001
Paxx$^{+/-}$ vs. *DNA-PKcs*$^{-/-}$	****	<0.0001
Paxx$^{-/-}$ vs. *Xlf*$^{-/-}$	ns	0.0512
Paxx$^{-/-}$ vs. *Ku80*$^{-/-}$	****	<0.0001
Paxx$^{-/-}$ vs. *DNA-PKcs*$^{-/-}$	****	<0.0001
Xlf$^{-/-}$ vs. *Ku80*$^{-/-}$	****	<0.0001
Xlf$^{-/-}$ vs. *DNA-PKcs*$^{-/-}$	****	<0.0001
Ku80$^{-/-}$ vs *DNA-PKcs*$^{-/-}$	ns	0.9994

[1] not significant (ns) = $p > 0.05$, * = $p \leq 0.05$, **** = $p < 0.0001$

Table C.5: Statistical analyzes of thymocyte cell count among WT, *Paxx*$^{+/-}$, *Paxx*$^{-/-}$, *Xlf*$^{-/-}$, *Ku80*$^{-/-}$, and *DNA-PKcs*$^{-/-}$ mice with indicated significance and *p*-values (one-way ANOVA).

Thymocyte cell count	**Significance**[1]	***p*-value**
WT vs. *Paxx*$^{+/-}$	ns	0.6475
WT vs. *Paxx*$^{-/-}$	ns	0.2808
WT vs. *Xlf*$^{-/-}$	**	0.0026
WT vs. *Ku80*$^{-/-}$	****	<0.0001
WT vs. *DNA-PKcs*$^{-/-}$	****	<0.0001
Paxx$^{+/-}$ vs. *Paxx*$^{-/-}$	ns	0.9614
Paxx$^{+/-}$ vs. *Xlf*$^{-/-}$	*	0.0261
Paxx$^{+/-}$ vs. *Ku80*$^{-/-}$	****	<0.0001
Paxx$^{+/-}$ vs. *DNA-PKcs*$^{-/-}$	****	<0.0001
Paxx$^{-/-}$ vs. *Xlf*$^{-/-}$	ns	0.1372
Paxx$^{-/-}$ vs. *Ku80*$^{-/-}$	****	<0.0001
Paxx$^{-/-}$ vs. *DNA-PKcs*$^{-/-}$	****	<0.0001
Xlf$^{-/-}$ vs. *Ku80*$^{-/-}$	ns	0.0546
Xlf$^{-/-}$ vs. *DNA-PKcs*$^{-/-}$	*	0.0315
Ku80$^{-/-}$ vs *DNA-PKcs*$^{-/-}$	ns	>0.9999

[1] not significant (ns) = $p > 0.05$, * = $p \leq 0.05$, ** = $p \leq 0.01$, **** = $p < 0.0001$

Table C.6: Statistical analyzes of bone marrow cell count among WT, *Paxx*$^{+/-}$, *Paxx*$^{-/-}$, *Xlf*$^{-/-}$, *Ku80*$^{-/-}$, and *DNA-PKcs*$^{-/-}$ mice with indicated significance and *p*-values (one-way ANOVA).

Bone marrow cell count	**Significance**[1]	***p*-value**
WT vs. *Paxx*$^{+/-}$	ns	>0.9999
WT vs. *Paxx*$^{-/-}$	ns	0.6893
WT vs. *Xlf*$^{-/-}$	ns	0.3642
WT vs. *Ku80*$^{-/-}$	**	0.0048
WT vs. *DNA-PKcs*$^{-/-}$	ns	0.2002
Paxx$^{+/-}$ vs. *Paxx*$^{-/-}$	ns	0.4417
Paxx$^{+/-}$ vs. *Xlf*$^{-/-}$	ns	0.2019
Paxx$^{+/-}$ vs. *Ku80*$^{-/-}$	**	0.0014
Paxx$^{+/-}$ vs. *DNA-PKcs*$^{-/-}$	ns	0.0998
Paxx$^{-/-}$ vs. *Xlf*$^{-/-}$	ns	0.9597
Paxx$^{-/-}$ vs. *Ku80*$^{-/-}$	*	0.0433
Paxx$^{-/-}$ vs. *DNA-PKcs*$^{-/-}$	ns	0.7858
Xlf$^{-/-}$ vs. *Ku80*$^{-/-}$	ns	0.2855
Xlf$^{-/-}$ vs. *DNA-PKcs*$^{-/-}$	ns	0.9971
Ku80$^{-/-}$ vs *DNA-PKcs*$^{-/-}$	ns	0.5716

[1] not significant (ns) = $p > 0.05$, * = $p \leq 0.05$, ** = $p \leq 0.01$

Table C.7: Statistical analyzes of body weight among WT, *Paxx*$^{+/-}$, *Paxx*$^{-/-}$, *Xlf*$^{-/-}$, *Ku80*$^{-/-}$, and *DNA-PKcs*$^{-/-}$ mice with indicated significance and *p*-values (one-way ANOVA).

Body weight	**Significance**[1]	***p*-value**
WT vs. *Paxx*$^{+/-}$	ns	0.7903
WT vs. *Paxx*$^{-/-}$	ns	0.3468
WT vs. *Xlf*$^{-/-}$	ns	0.9534
WT vs. *Ku80*$^{-/-}$	**	0.0065
WT vs. *DNA-PKcs*$^{-/-}$	ns	0.9803
Paxx$^{+/-}$ vs. *Paxx*$^{-/-}$	ns	0.9388
Paxx$^{+/-}$ vs. *Xlf*$^{-/-}$	ns	>0.9999
Paxx$^{+/-}$ vs. *Ku80*$^{-/-}$	*	0.0367
Paxx$^{+/-}$ vs. *DNA-PKcs*$^{-/-}$	ns	0.9999
Paxx$^{-/-}$ vs. *Xlf*$^{-/-}$	ns	0.9591
Paxx$^{-/-}$ vs. *Ku80*$^{-/-}$	ns	0.1547
Paxx$^{-/-}$ vs. *DNA-PKcs*$^{-/-}$	ns	0.9507
Xlf$^{-/-}$ vs. *Ku80*$^{-/-}$	ns	0.0736
Xlf$^{-/-}$ vs. *DNA-PKcs*$^{-/-}$	ns	>0.9999
Ku80$^{-/-}$ vs *DNA-PKcs*$^{-/-}$	ns	0.0817

[1] not significant (ns) = $p > 0.05$, * = $p \leq 0.05$, ** = $p \leq 0.01$

Appendix D: PAXX Western Blot

Western blot of PAXX (22kDa) in spleens and thymi isolated from WT, heterozygous, and knockout mice. Splenic and thymic WT samples are from the same mouse, splenic and thymic heterozygous samples are from the same mouse, and splenic and thymic knockout samples are from the same mouse. Knockout confirmed by the absence of PAXX protein in the splenic *Paxx*$^{-/-}$ sample. In addition, the genotypes were verified two times by PCR with independent tissue samples. The weak band observed in the thymic *Paxx*$^{-/-}$ sample is thus either unspecific or a result of spillover between wells during loading of the gel. The blot indicates that PAXX is expressed at higher levels in the thymus compared to the spleen, and that there is a reduction in PAXX protein levels in the heterozygous mouse compared to the WT.

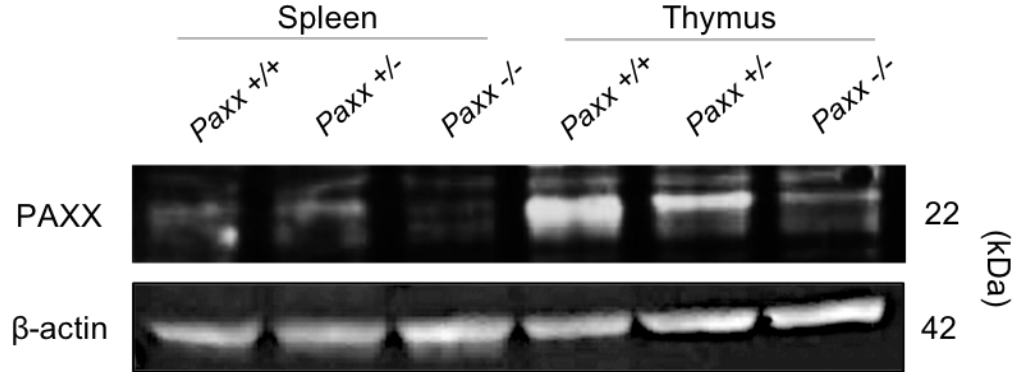

Appendix E: Flow Cytometric Analysis

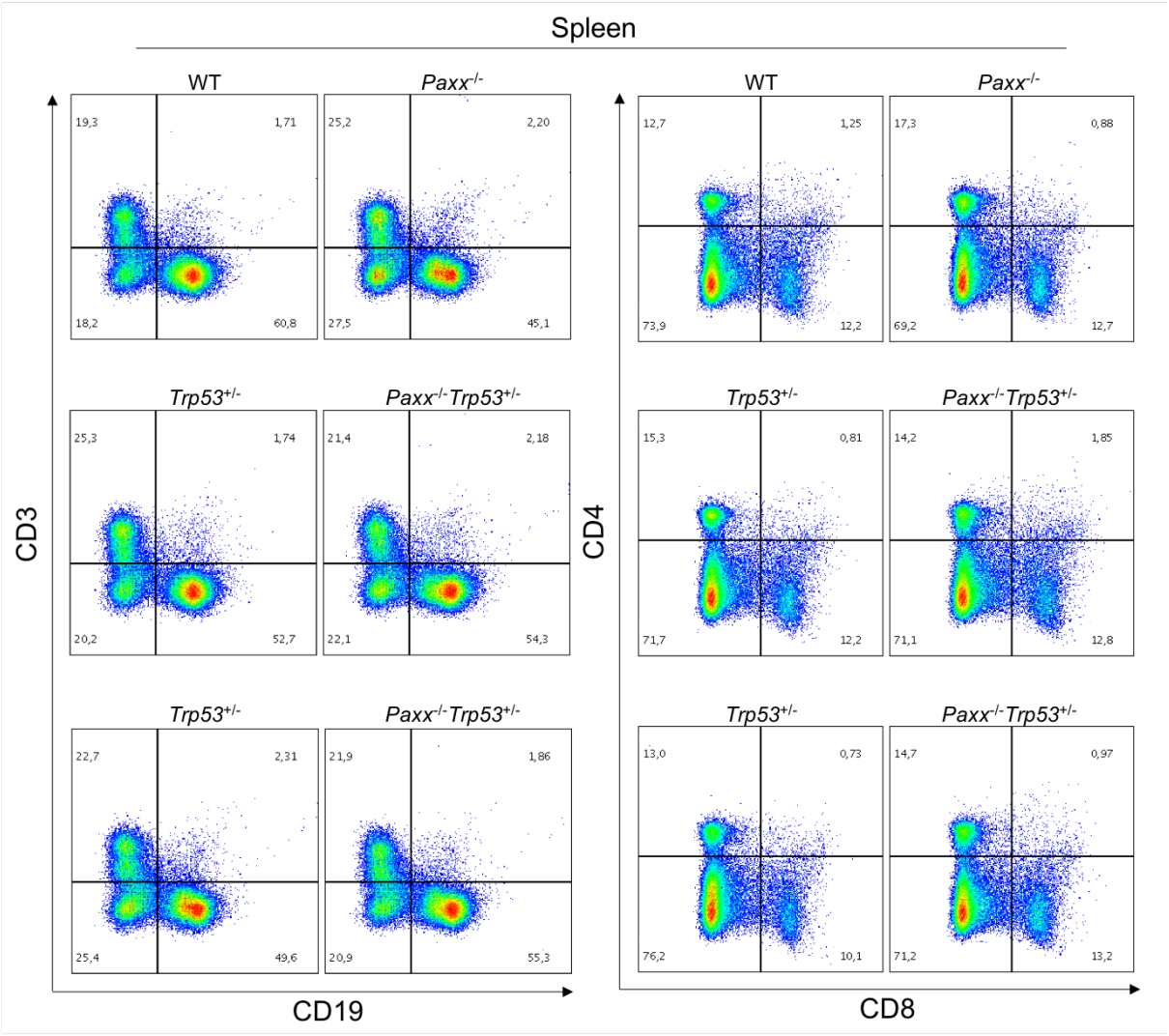

Figure E.1: Flow cytometric analysis of splenocytes isolated from WT and *Trp53*$^{+/-}$ (controls), *Paxx*$^{-/-}$, and *Paxx*$^{-/-}$*Trp53*$^{+/-}$ mice. **Left:** CD3^{+} and CD19^{+} of splenocytes with indicated genotypes and frequencies (%). **Right:** CD4^{+} and CD8^{+} splenocytes with indicated genotypes and frequencies (%).

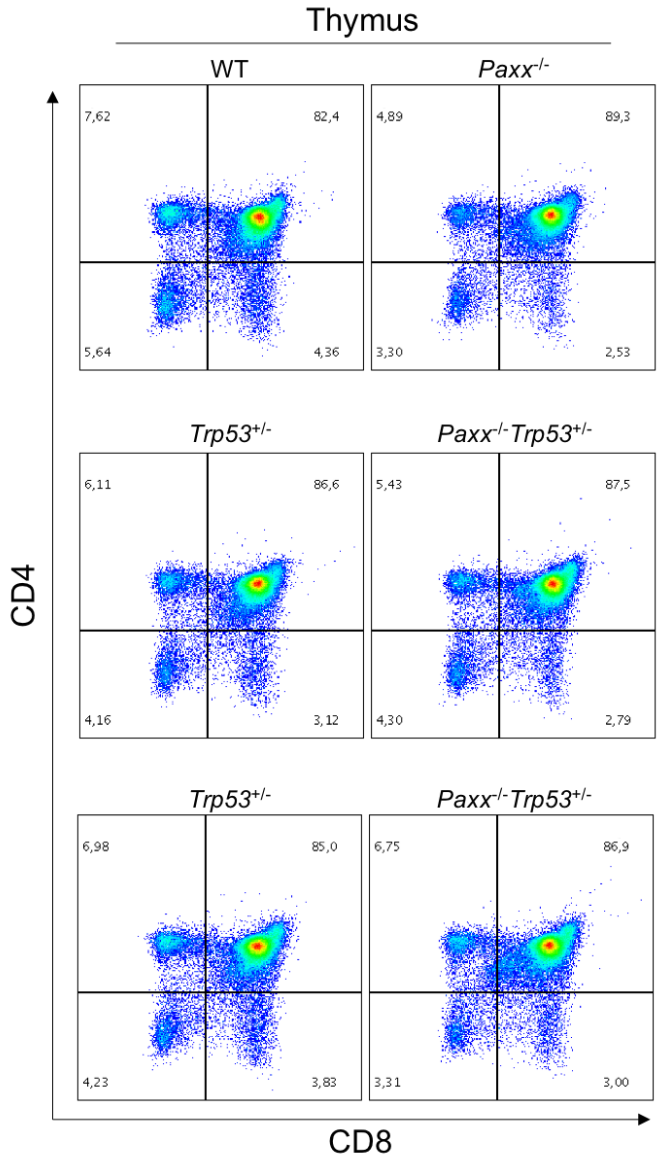

Figure E.2: Flow cytometric analysis of $CD4^+$ and $CD8^+$ thymocytes isolated from WT, *Trp53*$^{+/-}$, *Paxx*$^{-/-}$, and *Paxx*$^{-/-}$*Trp53*$^{+/-}$ mice. Genotypes and cell frequencies (%) are indicated.

Table E.1: Statistical analyzes of splenocyte frequencies among controls (WT and *Trp53*$^{+/-}$) and PAXX-deficient (*Paxx*$^{-/-}$ and *Paxx*$^{-/-}$*Trp53*$^{+/-}$) mice with indicated *p*-value and significance (t-test).

Spleen	
Comparison (Control vs. PAXX-deficient)	***p*-value, significance[1]**
$CD3^+$	0.8587, ns
$CD19^+$	0.5801, ns
$CD3^-CD19^-$	0.4917, ns
$CD4^+$	0.2422, ns
$CD8^+$	0.1224, ns
$CD4^-CD8^-$	0.0774, ns

[1] ns = not significant, $p > 0.05$

Table E.2: Statistical analyzes of thymocyte frequencies among controls (WT and *Trp53*$^{+/-}$) and PAXX-deficient (*Paxx*$^{-/-}$ and *Paxx*$^{-/-}$*Trp53*$^{+/-}$) mice with indicated *p*-value and significance (t-test).

Thymus	
Comparison (Control vs. PAXX-deficient)	***p*-value, significance[1]**
$CD4^-CD8^-$	0.1502, ns
$CD4^+CD8^+$	0.0851, ns
$CD4^+$	0.1602, ns
$CD8^+$	0.0604, ns

[1] ns = not significant, $p > 0.05$

Appendix F: Protein BLAST of Murine and Human p53, Isoform *a*

Protein BLAST comparing murine p53 isoform *a* (top) with human p53 isoform *a* (bottom), with a 77% identity and 82% similarity. Capital letters in the middle line indicate identical amino acids, spacing indicates different amino acids, and "+" indicates similar amino acids (see below). Amino acids that are different between the murine and human isoforms are highlighted in yellow.

```
Murine 4-57     MEESQSDISLELPLSQETFSGLWKLLPPEDIL-PSP-HCMDDLLL-PQDVEEFFE---GP
                MEE QSD S+E PLSQETFS LWKLLP  ++L P P   MDDL+L P D+E++F    GP
Human  1-60     MEEPQSDPSVEPPLSQETFSDLWKLLPENNVLSPLPSQAMDDLMLSPDDIEQWFTEDPGP

Murine 58-117   SEALRVSGAPAAQDPVTETPGPVAPAPATPWPLSSFVPSQKTYQGNYGFHLGFLQSGTAK
                 EA R+  A     P    P P APAPA  WPLSS VPSQKTYQG+YGF LGFL SGTAK
Human 61-120    DEAPRMPEAAPPVAPAPAAPTPAAPAPAPSWPLSSSVPSQKTYQGSYGFRLGFLHSGTAK

Murine 118-177  SVMCTYSPPLNKLFCQLAKTCPVQLWVSATPPAGSRVRAMAIYKKSQHMTEVVRRCPHHE
                SV CTYSP LNK+FCQLAKTCPVQLWV +TPP G+RVRAMAIYK+SQHMTEVVRRCPHHE
Human 121-180   SVTCTYSPALNKMFCQLAKTCPVQLWVDSTPPPGTRVRAMAIYKQSQHMTEVVRRCPHHE

Murine 178-237  RCSDGDGLAPPQHLIRVEGNLYPEYLEDRQTFRHSVVVPYEPPEAGSEYTTIHYKYMCNS
                RCSD DGLAPPQHLIRVEGNL  EYL+DR TFRHSVVVPYEPPE GS+ TTIHY YMCNS
Human 181-240   RCSDSDGLAPPQHLIRVEGNLRVEYLDDRNTFRHSVVVPYEPPEVGSDCTTIHYNYMCNS

Murine 238-297  SCMGGMNRRPILTIITLEDSSGNLLGRDSFEVRVCACPGRDRRTEEENFRKKEVLCPELP
                SCMGGMNRRPILTIITLEDSSGNLLGR+SFEVRVCACPGRDRRTEEEN RKK     ELP
Human 241-300   SCMGGMNRRPILTIITLEDSSGNLLGRNSFEVRVCACPGRDRRTEEENLRKKGEPHHELP

Murine 298-357  PGSAKRALPTCTSASPPQKKKPLDGEYFTLKIRGRKRFEMFRELNEALELKDAHATEESG
                PGS KRALP  TS+SP  KKKPLDGEYFTL+IRGR+RFEMFRELNEALELKDA A +E G
Human  301-360  PGSTKRALPNNTSSSPQPKKKPLDGEYFTLQIRGRERFEMFRELNEALELKDAQAGKEPG

Murine 358-390  DSRAHSSYLKTKKGQSTSRHKKTMVKKVGPDSD
                 SRAHSS+LK+KKGQSTSRHKK M K  GPDSD
Human 361-393   GSRAHSSHLKSKKGQSTSRHKKLMFKTEGPDSD
```